UNIVERSITI TEKNIKAL MALAYSIA MELAKA

CORRELATION OF CHARPY IMPACT BETWEEN WELDED AND UNWELDED MATERIAL

MUHAMMAD HAFIZIN ARIF BIN TAJUDIN

BACHELOR OF MECHANICAL AND MANUFACTURING ENGINEERING TECHNOLOGY (AUTOMOTIVE TECHNOLOGY) WITH HONOURS

2022

UNIVERSITI TEKNIKAL MALAYSIA MELAKA

Faculty of Mechanical and Manufacturing Engineering Technology

CORRELATION OF CHARPY IMPACT BETWEEN WELDED AND UNWELDED MATERIAL

MUHAMMAD HAFIZIN ARIF BIN TAJUDIN

Bachelor of Mechanical And Manufacturing Engineering Technology (Automotive Technology) with Honours

2022

CORRELATION OF CHARPY IMPACT BETWEEN WELDED AND UNWELDED MATERIAL

MUHAMMAD HAFIZIN ARIF BIN TAJUDIN

A thesis submitted
in fulfillment of the requirements for the degree of
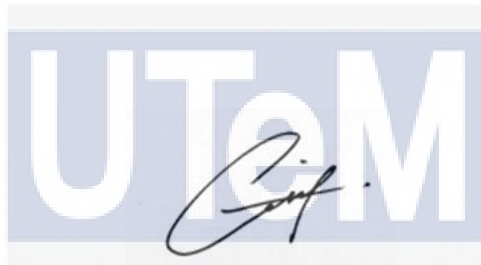**Bachelor of Mechanical And Manufacturing Engineering Technology (Automotive Technology) with Honours**

Faculty of Mechanical and Manufacturing Engineering Technology

UNIVERSITI TEKNIKAL MALAYSIA MELAKA

2022

DECLARATION

I declare that this Choose an item. entitled "Correlation Of Charpy Impact Between Welded And Unwelded Material" is the result of my own research except as cited in the references. The Choose an item. has not been accepted for any degree and is not concurrently submitted in candidature of any other degree.

Signature   :

Name   :   MUHAMMAD HAFIZIN ARIF BIN TAJUDIN

Date   :   11th June 2023

APPROVAL

I hereby declare that I have checked this thesis and in my opinion, this thesis is adequate in terms of scope and quality for the award of the Bachelor of Mechanical and Manufacturing Engineering Technology (Automotive Technology) with Honours.

Signature : *basri*

Supervisor Name : DR. MOHD BASRI BIN ALI

Date : 11 January 2023

DEDICATION

Every challenging work, needs self efforts, as well as guidannce of elders especially those who were very close to our heart. My humble effort I dedicated to my biggest supporter, my sweet, caring, loving parents,Mr. Tajudin bin Yusof & Mrs. Huzaimah binti Amirudin. Whose affection, love, encouragement and prays of day and night make me able to get success and honor. Not to forget my beloved siblings, Fatin Liyana, Amirah Fatanah, Idayu Farahin and Amirul Aiman for being helpful and supportive towards this journey, from start till end of this study. And finally, I would proudly dedicated to my life-sharing partner, Adibah Nur Athirah for expressing abundance of opinion and informative idea towards this thesis study.

ABSTRACT

This thesis investigates the effects of different parameters which is type of materials and material thickness on the results of energy absorption and impact strain signal behaviours due to Charpy impact test. Findings from Charpy impact test was used to investigate the correlation of absorb energy between welded and unwelded (based) material. This thesis also analyze the the study of impact signal between the welded and unwelded material. Hence, covers the study of material thickness effect on energy absorbtion. Mild steel is the common type of steel that used in automotive industry because of its material characteristics and low-cost manufacturing production. Due to its massive usage in the automobile parts, this steel must be design in variety ways to meet both crash safety and performance needs. Recently, the number of accident on highway has been increased due to loss of structure integrity to withstand high impact load. On collision, one of the concertrates matter is the joint of automobile parts especially body chasis which joint together by the welding process. This give an idea on how weld zone has effect the base material after the application of welding process and what is the effect of impact energy on weld zone compared to the base material. To better understand about this phenomenon, this study has to be done between two types of specimens which is welded material and unwelded material. These specimens must be test with the Charpy impact test, also known as the Charpy V-notch test to measure the amount of energy absorbed by the specimen during fracture. By the additional application of strain gauge, we can correlate the energy absorbed with strain energy by installing strain gauge to striker hammer that connected to data acquisition system (SOMAT eDAQ). Through the test we can also visualize the difference of impact signal between the welded and the unwelded material. Besides that, mechanical testing of tensile test with the same material is carried out to obtain the material behavior and to identify the material properties for additional and supporting data purpose.

ABSTRAK

Tesis ini bertujuan untuk menyiasat kesan parameter yang berbeza iaitu jenis bahan kajian dan ketebalan bahan kajian ke atas hasil penyerapan tenaga dan tindak balas isyarat terikan hentaman menggunakan ujian hentaman Charpy. Dapatan daripada kajian hentaman Charpy digunakan untuk menyiasat hubungkait serapan tenaga antara bahan yang dikimpal dan tidak dikimpal (bahan asas). Tesis ini juga menganalisis kajian isyarat hentaman antara bahan yang dikimpal dan tidak dikimpal. Justeru, mengkaji hubungan antara perbezaan ketebalan bahan terhadap penyerapan tenaga. Keluli lembut adalah jenis keluli yang biasa digunakan dalam sektor industri automotif kerana ciri-ciri bahan tersebut dan kos pengeluaran dan pembuatan yang rendah. Disebabkan penggunaannya secara meluas dalam pembinaan bahagian-bahagian kenderaan jalan raya, keluli ini mesti direka bentuk dalam pelbagai cara untuk memenuhi kedua-dua aspek dalam keperluan untuk keselamatan kemalangan dan prestasi memandu. Baru-baru ini, bilangan kemalangan di lebuh raya telah meningkat disebabkan kehilangan integriti struktur untuk menahan beban berimpak tinggi. Dalam perlanggaran, salah satu bahagian bahan yang difokuskan ialah sambungan bahagian-bahagian kereta terutamanya casis badan yang disambung menggunakan proses kimpalan. Ini memberi gambaran idea tentang bagaimana zon kimpalan memberi kesan terhadap bahan asas selepas aplikasi proses kimpalan dan apakah kesan tenaga hentaman ke atas zon kimpalan berbanding dengan bahan asas.Untuk lebih memahami fenomena ini, kajian ini perlu dilakukan antara dua jenis spesimen iaitu bahan yang dikimpal dan bahan tidak dikimpal. Spesimen ini mesti diuji dengan ujian hentaman Charpy, juga dikenali sebagai ujian takuk Charpy V untuk mengukur jumlah tenaga yang diserap oleh spesimen semasa patah. Dengan penggunaan tolok terikan, kita juga boleh menghubungkait tenaga yang diserap dengan tenaga terikan dengan memasang tolok terikan pada tukul hentaman dan disambungkan dengan sistem pemerolehan data (SOMAT eDAQ). Melalui ujian tersebut, kita juga boleh meneliti perbezaan isyarat hentaman antara bahan yang dikimpal dan yang tidak dikimpal. Selain itu, mekanikal ujian tegangan dengan bahan yang sama dijalankan untuk mendapatkan bacaan kebolehan bahan dan mengenal pasti sifat bahan untuk tujuan data tambahan dan sokongan.

ii

ACKNOWLEDGEMENTS

TABLE OF CONTENTS

LIST OF TABLES

LIST OF FIGURES

LIST OF SYMBOLS AND ABBREVIATIONS

ABBREVIATIONS

CVN	-	Charpy V-notch
ASTM	-	American Society for Testing and Materials
SAE		Self-addressed Envelope
HAZ	-	Heat Affected Zone
ISO	-	International Organization for Standardization
PSD	-	Power Spectrum Density
PE	-	Potential Energy
KE	-	Kinetic Energy
KV		Notch Impact
SEB		Single Edge Bend
BH		Bake Hardening
IF		Interstitial Free
MA		Martensite Austenite
HSLA		High-strength Low-alloy Steel
HSS		High-strength Steel
AHSS		Advance High-strentgh Steel
TBF		TRIP Aided Banatic Ferrite
SMAW		Shielded Metal Arc Welding
FCAW		Flux Cored Arc Welding
GMAW		Gas Metal Arc Welding
GTAW		Gas Tungsten Arc Welding
MIG		Metal Inert Gas
TIG		Tungsten Inert Gas
PWHT		Post-weld Heat Treatment

SYMBOLS

A	Area
ε	Strain
E	Young Modulus

F	Force
J	Impulse
k	Spring stiffness
M	Total mass
ms	miliseconds
v	Velocity
σ	Stress
r	Radius
m	Mass
h	Height
H	Total height
V	Knotch impact
L	Length
ΔL	Elongation
D	Diameter
c	Damper of viscous damping coefficient
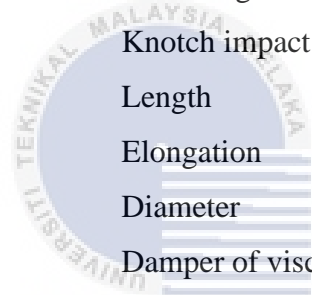
LIST OF APPENDICES

xii

CHAPTER 1

INTRODUCTION

1.1   Background

The automotive sector is critical to the economies of developed countries. Due to the increasing worldwide rivalry, one of the primary goals in the automobile industry is low-cost manufacturing. As the least expensive of all steels and the most widely used, mild steel is the most optional alloy for an industry that's going to works with hefty amounts of metal. This is why it's so commonly used by the automotive business for chassis and body panels in every road-worthy vehicle. Mild steel has advantages over other metals and materials in the automobile industry, and its versatility is something that has a profound cost-benefit that can also be developed for future industrial usage. Concerning the recent trends in car production, the application of lightweight constructions principles is the main priority to meet customers' demands and the increased legal requirements. To meet these expectations, the application of high strength materials is regarded as one of the most promising possibilities. Mild steel not only meets a car manufacturer's desire for light-weight vehicles, but it also helps the (essential for making automobiles as fuel efficient as feasible). It is, nevertheless, quite cost effective and could be constructed in such a number of ways to meet both collision safety and performance requirements. Mild steel's elasticity does not compromise its ability to absorb the energy in the case of a collision. In terms of safety, it should go without saying that impact resistance is critical in the vehicle business. In automotive and other safety-critical industries, impact testing is a vital evaluation of a material's failure qualities and useful tool for determining a material's failure properties.

13

Engineers can prevent failures, develop long-lasting items, and save lives by properly testing raw materials and molded components for strength and durability. For better understanding and study of impact testing on automotive industry, Charpy Impact Test is the most commonly used test to evaluate the relative toughness of a material in a fast and economic way. The Charpy impact test was invented in 1900 by Georges Augustin Albert Charpy (1865–1945), and still in used in many industries for testing materials today. The Charpy impact test measures the energy absorbed by a standard notched specimen while breaking under an impact load which is used for determining the amount of forces that are absorbed by materials when it reaches the point of fracture. The Charpy Impact Test can be used to determine the malleability and ductility of a material that is being forged or produced for the parts of the automobile.

One of the most concentrates matter of impact tensile test in automotive industry is a result of experiments obtained on the different welded steel grades by means of the new developed automobile products. This including two aspects; 1) State of the art concerning joining techniques for automotive industry and 2) State of the art concerning dynamic testing of high strength welds for automotive industry (Bayraktar et al., 2009) [1]. Frames, channel, angle, as well as plates are among the welded construction methods steel structures used in automobiles. Bolts, welded connections, or rivets are then used to attach them together. These structures in automobiles are frequently subjected to loads, and they can exceed their design load. It must be in service for an extended period of time and must fight with environmental and service conditions that may cause changing strains. A steel piece that is part of the structure, such as a car chassis or bodyframe, will have a structural function that is independent of the rest of the structure. That most of these component pieces are welded together, adding to the application's toughness, durability, and longevity. Steel structures

then were going to be subjected to varying stresses as a result of vehicle loads, road conditions, or driving style, and can experience fatigue failures as a result of the weld.

A research of (Barbosa et al., 2021)[22] provided a fracture testing program that measured cleavage fracture toughness data for welded steel by using various welding procedures with in ductile to brittle transition region. Verification studies of the correlation between CVN energy and fracture strength and hardness for trialed weldments formed by the SMAW as well as FCAW processes may provide nonconservative integrity assessment for imperfect structural parts because the calculated impact strength values are greater than the result test values. More addition research (Kunigita et al., 2020)[23], the findings of Charpy impact testing for a variety of simulated heat-affected zone (HAZ) samples with various chemical compositions and temperature cycles on weld specimen. The results shown different microstructural parameters HAZ does give an effect on absorb energy of the specimen.
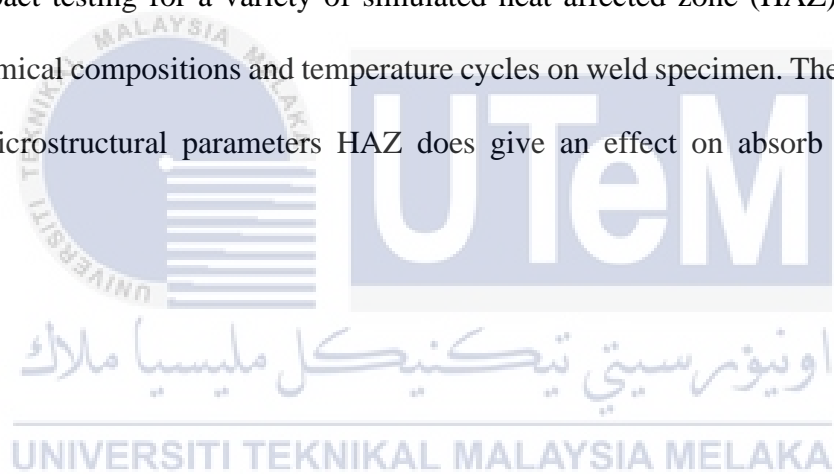
1.2   Problem Statement

Welding process does bring an impact or effect on the material. According to the research (Thomas, 2018) [2], on a certain parameter, types of welding or even welding skills can cause changing of metal microstructure and its mechanical properties. Failure of welded construction steel components can occur due to inappropriate design, wrong steel choice or quality, substandard welding processes and through defective maintenance. The degree of deformation before the creation of a brittle crack varies significantly for metals with varied microstructures. It is demonstrated that the metal of welded joints is destroyed with a considerable amount of energy consumed on the ultimate fracture of the specimen relative to the base metal (Sudin et al., 2020) and (Kim et al., 2015) [11-12]. (Barbosa et al.,2021) [22] developed a fracture testing methodology for steel welds in the ductile-to-brittle transition area that assessed cleavage fracture toughness data. Because the calculated toughness values are greater than the experimentally measured values, verification investigations of the link between CVN energy and fracture toughness may give nonconservative integrity assessment for defective structural components. In addition, the outcomes of Charpy impact testing for a variety of simulated heat-affected zone (HAZ) samples with varying chemical compositions and temperature cycles on weld specimens (Kunigita et al., 2020) [23]. The results reveal that different microstructural factors HAZ have an effect on the specimen's absorb energy. Furthermore, according to the research (Sudin et al., 2020) and (Kim et al., 2015) [11-12], the behavior of welded joints and low-alloy low-carbon steel during impact bending is investigated from the standpoint of energy partitioning due to the crack formation process. It states that, there are significant variances in the degree of deformation preceding the creation of a brittle crack for metals with varying microstructures.

16

To better understand about this phenomenon, a study has to be done between two types of specimens which is welded material and unwelded material. These specimens must be test with the Charpy impact test, also known as the Charpy V-notch test to measure the amount of energy absorbed by the specimen during fracture. Through this test we can calculate and observe the amount of energy absorb by both of the specimens and also can visualize the difference of impact signal between them. At the end of the test, we can finally conclude that whether the welding process does give an effect on the material in certain characteristic compared to the unwelded material.

1.3   Research Objective

The main aim of this research is:

a)   To study weld impact testing in automotive application

b)   To correlate the absorb energy between welded and unwelded material.

c)   To analyze the impact signal between welded and unwelded material.

1.4   Scope of Research

The scope of this research are as follows:

- There are two types of specimens which is welded and unwelded material using mild steel material follow ASTM E23 standard with different thickness.

- The machine that is used is a Pendulum Charpy Impact machine testing maximum capacity 500J (Jinan Precision JBW-500).

- Impact velocity Charpy impact machine 5.4 m/s.

- Using shielded metal arc welding (SMAW) process to produce CVN welded material specimen

17

CHAPTER 2

LITERATURE REVIEW

2.1   Impact

In physics, collision, the sudden, forceful colliding of two bodies in immediate touch also called impact There are three types of collisions between two bodies: linear central impacts, oblique central impacts, and eccentric impacts (Oztas A.G., 1999) [3]. In highway collisions, eccentric impact is more common than other types of impact. When the energy of an impact is transferred from one person or item to another, it is called collision. This wave of energy has the potential to injure or damage those who are affected, as well as items. The impact's cumulative effect, such as changes in mass velocities, is frequently calculated using the concept of a big force acting over a short period of time. To simplify the study of impulsive motion of two masses during contact, a concept of a large force operating for a short time is used. The average force of impact can be determined from the momentum exchange between the masses when the impact time is known (Rajalingham & Rakheja, 2000) [4].
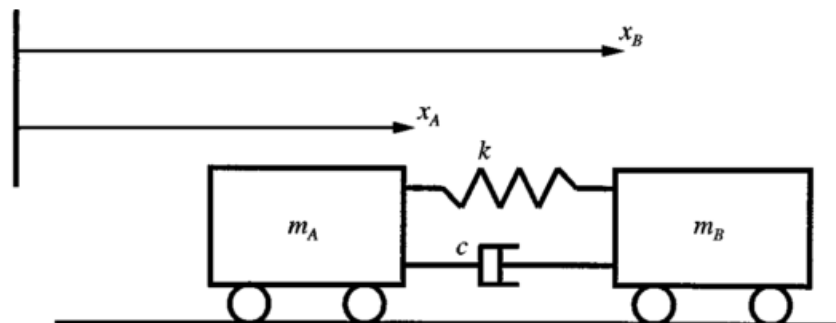
Figure 2.1: Model of mechanical system in collision between two masses (Rajalingham & Rakheja, 2000) [4]

Whenever two or many bodies collide, a large force or shock is applied during a short period of time, which is known as an impact in mechanics. A greater force delivered over a proportionally longer period has a greater effect than a smaller force acting over a shorter time period. The effect is highly reliant on the bodies' relative velocity in relation to each other. (Goldsmith W., 2001) [5]. An object struck by a projectile will deform at normal speeds during a perfectly inelastic collision, and this deformation will absorb most or all of the force of the collision. From the standpoint of energy conservation, the projectile's kinetic energy is converted into heat and sound energy as a result of the deformations and vibrations caused in the struck item. These deformations and vibrations, however, are not instantaneous. A high-velocity collision (an impact) does not provide these deformations and vibrations enough time to occur. As a result, the struck material acts as if it were more brittle than it could be, and the majority of the applied force is used to fracture it (Johnson et al., 1993) [6].

2.1.1 Impact and Energy

The conservation of energy is a basic concept in physics. "Energy is neither created nor destroyed; it is only converted from one form to another"- Albert Einstein, 1907. When a body's energy (and, eventually, the food you've consumed) is utilize to pick up a ball from the ground, it converting that energy into gravitational potential energy; when it releases, that same energy becomes kinetic (moving) energy. When the ball hits the ground, some of the energy is released as sound, and some may cause the ball to bounce back up. This notion is critical when calculating the energy and force of a falling item. Because of the law of conservation of energy, it is simple to calculate how much kinetic energy an object possesses right before impact. The energy has all come from the gravitational potential it had before

falling, hence the gravitational potential energy formula provides all the information it needs (Banas T.,2020) [18].

$$E = mgh \tag{2.1}$$

In the equation, m is the object's mass, E is its energy, g is the acceleration due to gravity (9.81 m s2 or 9.81 meters per second squared), and h is the height from which the object falls. It can simply calculate this for any falling object if know how big it is and how high it falls from.

2.1.2 Impact and Work

According to the work–energy principle, an increase in a rigid body's kinetic energy is caused by an equivalent amount of positive work done on the body by the consequent force exerted on that body. A decrease in kinetic energy, on the other hand, is generated by an equal amount of negative work done by the resulting force. As a result, if the network is positive, the particle's kinetic energy is increased by the amount of work. If the net work done is negative, the kinetic energy of the particle is reduced by the amount of work (Banas T.,2020) [18]. When calculating the falling object force, the work-energy principle is the final piece of the puzzle. According to this principle, equation 2.2.

Eaverage impact force× distance traveled= change in kinetic energy   (2.2)

Because this problem requires the average impact force, rearranging the equation yields. Equation 2.3 are as below.

$$\text{average impact force} = \frac{\text{change in kinetic energy}}{\text{distance travelled}} \qquad (2.3)$$

The sole remaining piece of information is the distance travelled, which is just how far the thing travels before coming to a stop. The average impact force is reduced if it enters the ground. This is sometimes referred to as the "deformation slow down distance," and it can be used when an object deforms and comes to a stop, even if it does not penetrate the ground. The whole formula can be stated as follows, using the distance travelled after impact as d and noting that the change in kinetic energy is the same as the gravitational potential energy as shown in equation 2.4 below.

$$\text{average impact force} = \frac{mgh}{d} \qquad (2.4)$$

2.1.3 Impact on Pendulum

According to the study, (Britannica T.,2021) [7] the principle of physics that states that the energy of interacting things or particles in a closed system remains constant. Kinetic energy, or energy of motion, was the first type of energy to be identified. The sum of the kinetic energy of the particles before collision equals the sum of the kinetic energy of the particles after collision in certain particle collisions known as elastic collisions. The concept of energy was gradually broadened to include various types. The kinetic energy lost by a body slowing down as it travels upward against gravity was thought to be turned into potential energy, or stored energy, which is then converted back into kinetic energy as the body accelerates during its return to Earth.

When a pendulum swings upward, for example, kinetic energy is transformed to potential energy. When the pendulum briefly stops at the top of its swing, its kinetic energy is zero, and the entire system's energy is in potential energy. The potential energy is

21

transformed back into kinetic energy when the pendulum swings back down. The total of

potential and kinetic energy is constant at all times.
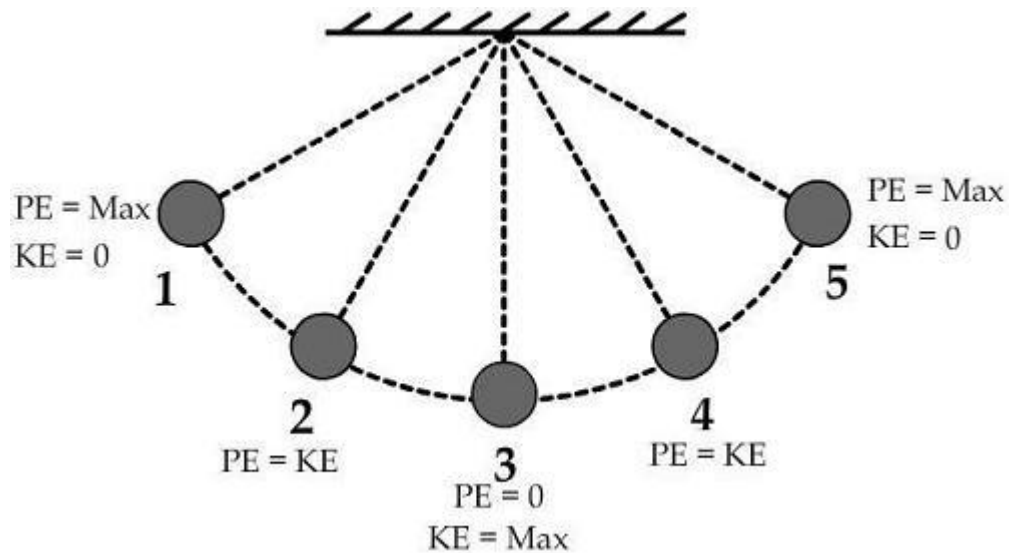
Figure 2.2: Potential energy and kinetic energy on pendulum.

2.2   Charpy V-notch Impact Test

The Charpy impact test, also called the Charpy V-notch test (CVN), is a standardized

high strain-rate test that assesses how much energy a material absorbs during fracture. This

absorbed energy is a measurement of a material's notch toughness and can be used to

investigate temperature-dependent ductile–brittle transitions. It is frequently used in industry

since it is simple to prepare and carry out, and results may be acquired fast and cheaply. S.B.

Russell (1898, American) and Georges Charpy invented the test in 1900. (1901, French).

Because of Charpy's technical contributions and standardization efforts, the test became

known as the Charpy test in the early 1900s. This test determines the resistance of a material

to impact from a swinging pendulum.

Based on the study (Ashter, 2014) [9], the Charpy impact test is used to determine

the resistance of plastics to breakage by flexural shock according to standard test method

ASTM D6110. It calculates how much energy is required to break standard test specimens

under certain specimen, mounting, notching, and pendulum velocity at impact conditions. A base holds a pair of supports that hold the specimen in the pendulum impact machine. As in the Fig 2.4, these supports are linked by a rigid frame and bearings, one of many pendulum-type hammers with a specific beginning energy for usage with a specific specimen, a pendulum holding and release mechanism, and a system for showing the specimen's breaking energy. The specimen anvil, pendulum, and frame are robust to keep the striking edge and specimen aligned correctly at impact and during fracture propagation, as well as to reduce energy losses due to vibration.
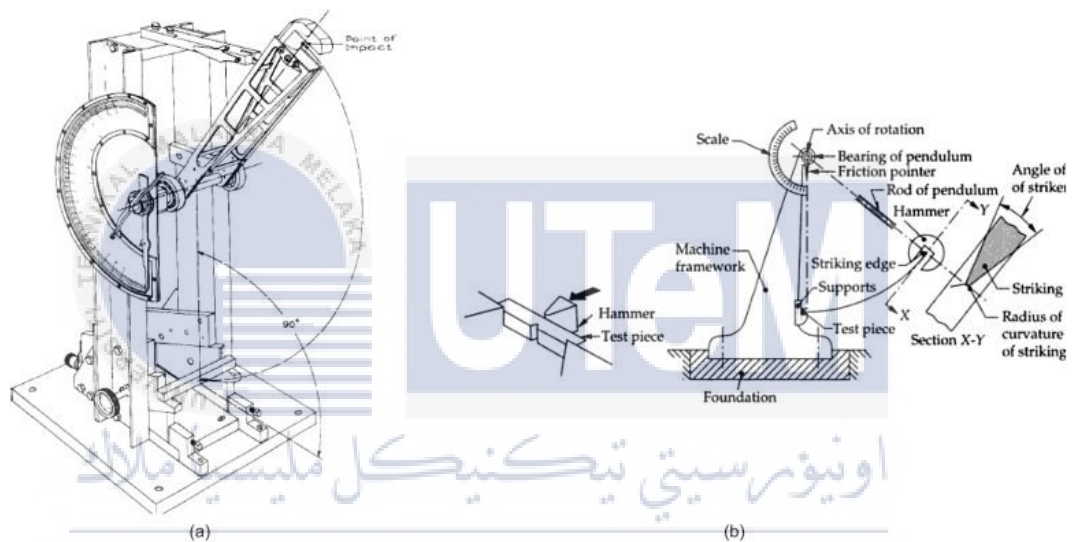
Figure 2.3: Configuration of Charpy V-notch Impact Test (Ashter, 2014) [9]

2.2.1 Impact on CVN

A Charpy impact test determines the resistance of a metal specimen to a instantaneous impact load applied by the pendulum swinging from such a given height. Using the force of a pendulum load, the Charpy test is used to estimate how much energy is required to break a metal object. The main purpose of the test is to see if the specimen is brittle or ductile. Brittle materials would be those who shatter without deforming plastically (no energy absorption). Ductile materials are ones that shatter when subjected to a large

23

amount of plastic deformation (low energy absorption). The Charpy machine must be calibrated at first. To do so, the dial gauge must be set to the highest value measurement and release the pendulum without the specimen. When the needle has now returned to the zero position, the Charpy machine is ready for testing. Then, at the end value, turn the dial gauge indication needle lower, set the specimen, and the pendulum swings down and slices the specimen when the pendulum is released. The pendulum does not reach full height on the other side due to the specimen's energy absorption. It can measure the quantity of energy absorbed by the specimen by using the dial gauge (in terms of Joules or Nm). the amount of energy absorbed by the test specimen to break is called Notch impact energy. Below is the figuration and equation of Notch impact energy respectively.
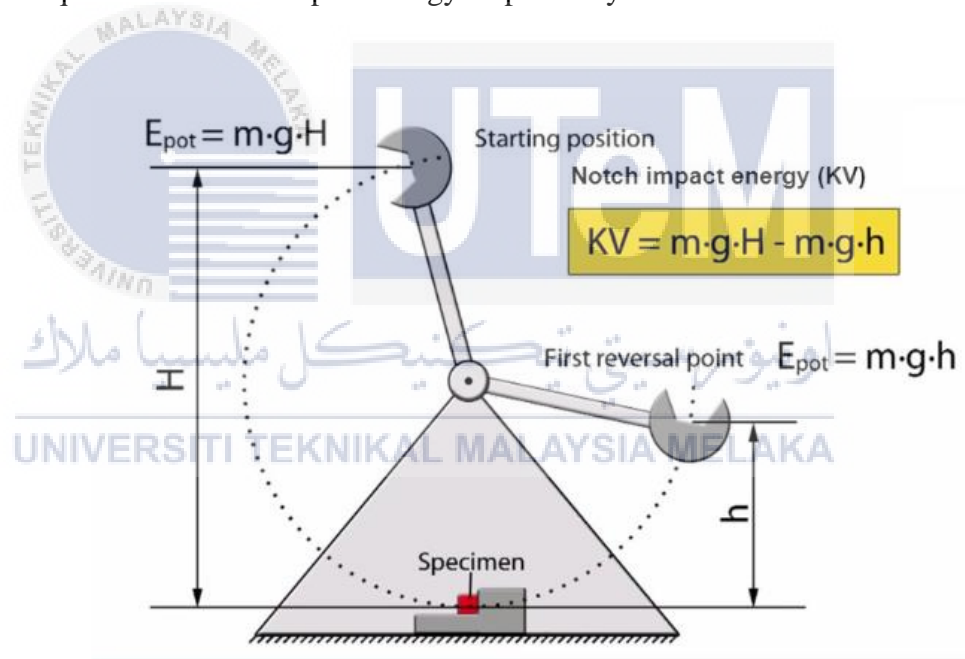
Figure 2.4: Configuration of CVN

$$KV = mgH - mgh \qquad (2.5)$$

Where;

m – Mass of the pendulum

g – Gravity

24

H – Height of Pendulum starting point

h – Height of the pendulum from the first reversal point

The energy required to shatter a typical test piece (specimen) under an impact load is known as impact energy. The Charpy impact test is the most frequent method of determining impact energy. Using a dial indicator of the change in pendulum height before and after the impact, the amount of absorbed energy in breaking the specimen is estimated. In alloys having high maximum and yield strength, and ductility (percentage of elongation in fracture region) values, impact fracture energy are high. Other methods of proving Charpy fracture energy have been utilised, such as kinetic energy changes measured during and after fracture using velocity measurements. Equation 2.6 gives the impact velocity when the pendulum impacts at the specimen refer position (2) (as indicated in Figure 2.6).
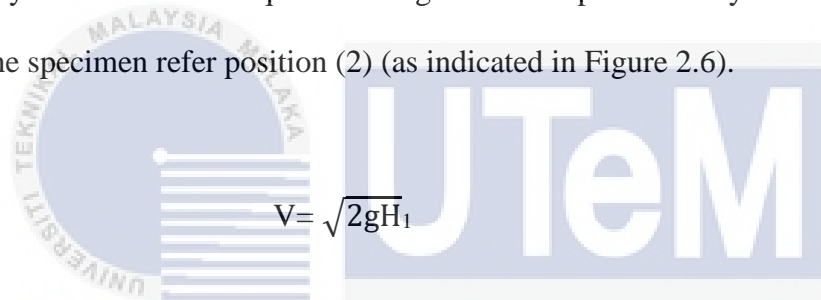
$$V = \sqrt{2gH_1} \qquad (2.6)$$

Where g is the acceleration of gravity and H is the difference in elevations of the center of contact. According to Equation 2.7, the energy acquired by the specimen when it breaks (i.e., the impact energy) indicates a loss of energy towards the pendulum. As a result, the change of the pendulum's potential energy between zero velocity locations (1) and (3), as shown in Figure 2.6, can be utilized to determine this loss.

$$U = mg\,(h, - h3\,) = mgr\,(\cos ß - \cos a) \qquad (2.7)$$

Where m indicates the pendulum mass and h1 and also h3 is the mass center altitudes. Furthermore, the center of mass is r degrees away from the center of rotation. (Ali et al., 2015) [24].
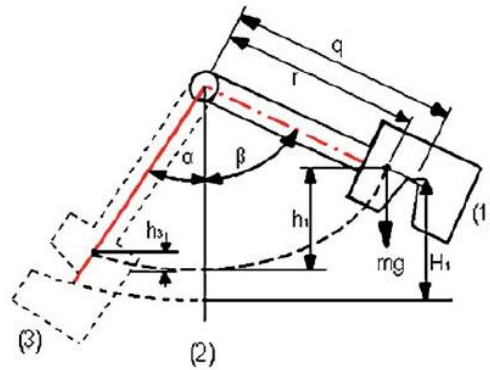
Figure 2.5: Charpy impact absorbed energy theory sketch (Ali et al., 2015) [24].

2.2.2   Strain Gauge

Many practical scenarios in engineering require understanding of the stresses and strains that are applied in a structure, because the predictability of the materials is heavily dependent on these factors (Silva et al., 2019) [25]. Strain is defined as the amount of deformation of a material experience due to an applied force as illustrated in Figure 2.7 and expressed Equation 2.8 below.
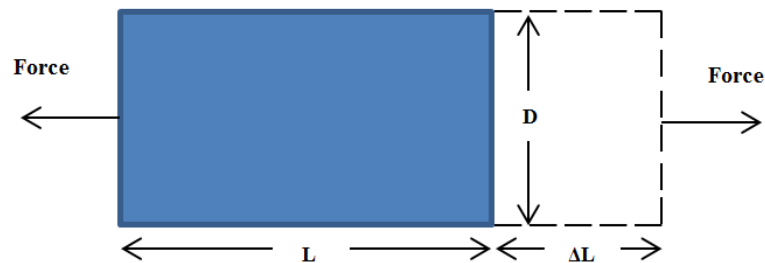
Figure 2.6: Deformation of Strain.

$$\text{Strain, } \varepsilon \frac{\Delta L}{L} \tag{2.8}$$

Tensile strain occurs when the length grows as a result of tensile stress. Compressive strain occurs when the length reduces owing to compressive stress. Volume strain is the ratio of a body's change in volume to its initial volume. Shear strain, on the other hand, is the strain caused by shear stresses. In this situation, the body moves transversely from its initial location. Shear strain is defined as the transverse shear displacement divided by the initial length. Below is the volume and shear strain Equation 2.9 and 2.10 depicted respectively.

$$\text{Volume strain } = \frac{\text{Change in Volume, } \Delta V}{\text{Original Volume, V}} \tag{2.9}$$

$$\text{Shear strain } = \frac{\text{Transverse shear displacement}}{\text{Original Length}} \tag{2.10}$$

Strain can be measured in a variety of ways, the most common of which is with a strain gauge. A passive transducer, such as a strain gauge, translates mechanical displacement into a change in resistance. Foil strain gauges, wire strain gauges, and semiconductor strain gauges are the three types. Mostly, many of the strain gauges are made of foil and are available in a number of forms and sizes to suit a variety of applications. Figure 2.8 depicts the structure of a foil type strain gauge. The strain gauge is usually affixed to the measuring object with glue. The glue and resin base transfer strain from the measuring point to the strain detecting element. The gauge factor, which is a quantitative expression of the strain gage's sensitivity to strain, is a crucial parameter of the strain gauge (GF).

27
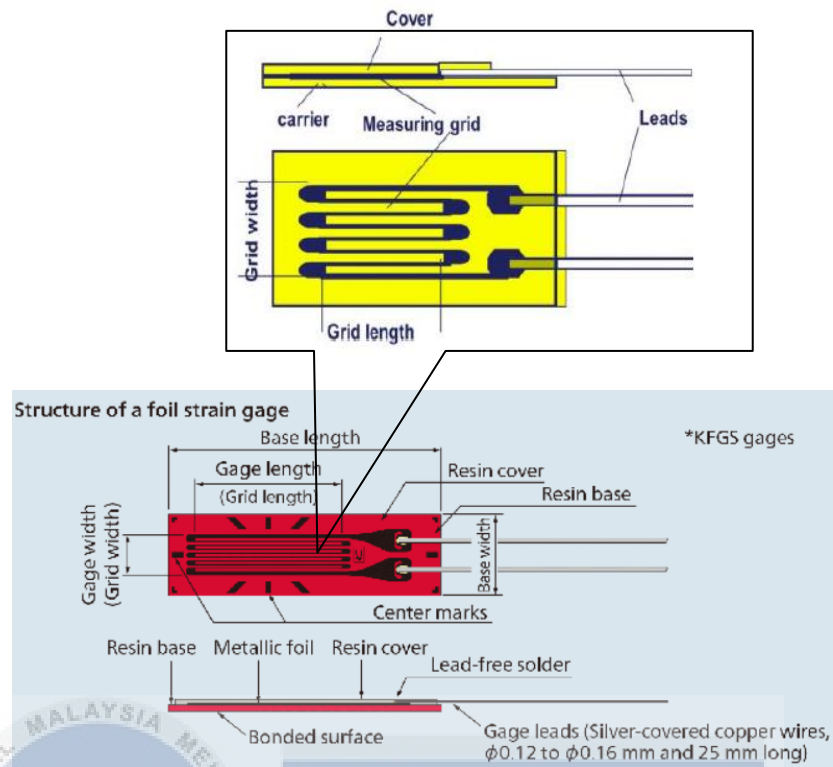
Figure 2.7: Structure of a foil type strain gauge.

The dynamic reactions of a conventional Charpy impact instrument were tested experimentally using strain gauges and an accelerometer coupled to the impact striker. Finite element analysis was used to validate the results (FEA) (Shterenlikht et al., 2005) [26]. When compared to strain gauges, the results demonstrate that the initial natural frequencies of the Charpy sample have significant modal magnitudes in the acceleration signal. Furthermore, a multichannel system of high-speed stresses and the load recording method during fracture toughness testing were investigated by (Kondryakov et al., 2005) [27]. Strain gauges fitted to the striker and specimen support can capture data on specimen deformation during the test. The variations in energy determined by dial/encoder energy versus an instrumented striker were investigated (Rittel et al., 2002) [28]. They measured vibration energy which called accelerometer data and applied Fourier analysis to calculate instrument striker energy, which is affected or linked to absorbed energy. According to (Rittel et al., 2002) [28] by using

28

internal and reference stresses, the impact strain energy acting to specimens can be determined.

2.2.2.1 Strain Signal

A signal is a set of numbers derived from a measurement taken as a function of time using a recording method. It's usually measured with an analogue-to-digital converter that generates an experimental signal at regular intervals. Deterministic and nondeterministic signals, as well as random signals, can be classified. A mathematical relationship between the function value and the time value is described as a deterministic signal. The signal can be further characterised to determine if it is periodic or non-periodic. Many signals in nature have nondeterministic or unpredictable features, which make signal processing methods difficult to analyse. A signal that represents a random event can be stationary or non-stationary.

Based on the research (Ali et al., 2015) [24] shows the relationship between the impact energy acquired from the laboratory test and the energy computed using the power spectrum density technique. According to a prior study, depending on the strength and ductility of the test material, the total absorbed energy obtained using the dial/encoder system could be significantly different. As a result, we used a signal processing approach to quantify the energy of the experimental system resulting from the dial/encoder Charpy impact test. At varying velocities and thicknesses, the energy absorbed throughout the experiment is compared to the strain energy.

A polynomial equation with R of 99.8% can be used to relate the total energy absorbed by the dial/encoder system. As a result, the energy from PSD is associated with the effect of the strain signal pattern and impact time with varying velocities and thicknesses.

Table 2—The PSD peak ($\mu\varepsilon^2$/Hz) and different percentage with different velocities and thicknesses				
Exp. no.	Velocity 5.18 m/s		Velocity 3.35 m/s	
	10 mm thickness (G1)	5 mm thickness (G2)	10 mm thickness (G3)	5 mm thickness (G4)
1	179.6	30.07	503.9	84.34
2	164.4	19.49	583.2	77.08
3	156.8	28.31	618.1	78.82
4	112.9	25.38	522.6	93.41
5	123.5	38.21	776.9	90.95
Average	147.4	28.3	600.9	84.9
% Differrence	421%	0%	2023%	200%

Figure 2.8: PSD peak and different percentage with different velocities and

thicknesses (Ali et al., 2015) [24].
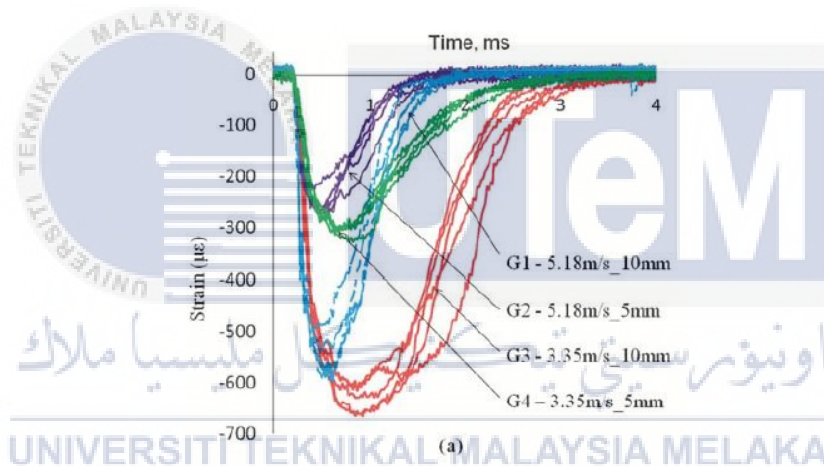
Figure 2.9:Strain signal plot of G1, G2, G3 and G4 thicknesses (Ali et al., 2015)

[24].

Charpy's impact has been instrumented. The PSD measure is based with the strain and the impact time value, according to the experimental results. Whenever strain and impact time are both high, PSD value will be higher. The absorbed energy is affected by velocity and thickness. Therefore, this parameter is crucial when testing the material. According to our findings, this material is easily damaged and fractured at higher velocity and lower thickness when compared to lower velocity and higher thickness.

As indicated by the polynomial relationship with R square of 99.8% between PSD energy and energy absorb, the higher the energy received, the greater the strain energy. This means the energy absorption is proportionate to the calculated strain energy from the PSD area. This correlation can replace the dial/encoder absorbed energy with energy using a signal processing method.. This discovery further confirms the appropriateness of PSD strain energy and implies that, in addition to the Charpy impact test, other studies can be performed to reliably validate impact energy.

2.2.3 CVN Specimen

The Charpy impact test evaluates the amount of energy absorbed by a standard notched specimens while breaking under impact stress. This type of test is still used as a low-cost technique of quality control for determining engineered materials such as metals, ceramics, composites, and polymers have notch sensitivity and impact toughness. Based on the research (Saba et al., 2019) [10] it performs a normal Charpy impact test which specimen 55 mmx 10 mmx10 mm in dimension which has a notch machined into it. When a regular notched specimen breaks under an impact load, the Charpy impact test is used to measure how much energy it absorbs. A suitable specimen is struck with a hammer on a pendulum arm while it is firmly held across both ends throughout this procedure. The hammer strikes the notch on the opposite side. By measuring the pendulum arm's reduction in motion, the quantity of energy absorbed by the material is precisely computed. Climatic conditions, high strain levels (due to impact or pressurized), and stress point focus like notches, cracks, and voids all have a role in a material's toughness.

2.2.4 Weld on CVN Specimen

According to (Sudin et al., 2020) and (Kim et al., 2015) [11-12], the behavior of welded joints and low alloy and low carbon steel during impact bending is investigated

through the standpoint of partitioning of energy which due to the fracture formation process. It states that, there are some variances in the certain deformation degree preceding the creation of a brittle fracture for metals with varying microstructures. The effort done before a brittle crack form as well as the almost every of fracture are proven to be linked. Statistical evidence is offered to support the increased vulnerability of welded joint metal to early brittle crack formation. It is shown that the metal of welded joints is damaged, with a significant amount of energy expended on the specimen's ultimate fracture relative to the base metal. The base metal from which a welded metal structure is constructed, as well as the metal of the welded connections, have an impact on its reliability. Metal constructions are frequently destroyed as a result of the inadequate reliability of metal welds.

Numerous procedures have been devised to measure the material's brittle fracture resistance under impact stress, as described in (Otani M.,1957) and (Hartbower C.E.,1963) [13-14]. The material is in the ductile to brittle transition temperature range, as evidenced by brittle fractures seen during impact bending testing. At the same time, the presence of a brittle crack during the deformation process significantly reduces the material's ability to withstand further crack propagation, because of a reduction in cross-section and the development of a powerful stress concentration.

Furthermore, the main issue with this type of dissimilar junction in weldment is the creation of localized strains at the interface related to thermal expansion coefficient (TEC) mismatch, development of heterogeneous microstructures along weldments, carbon diffusion which causes the creation of a carbon redundant, and carbon enriched hard zone near the contact. The issue related during the joining stage and at elevated temperature service condition causes the welds joint to fail prematurely at service condition. The

selection of the filler metal is one of the main issues for making the dissimilar joint of the weld between two steels (Sirohi et al., 2021) [15].

2.2.5 Impact on Welded Material

A research of (Barbosa et al., 2021) [22] provided a fracture testing programmed for ASTM A572 Grade 50 steel welds manufactured using various welding methods in the ductile-to-brittle transition area that measured cleavage fracture toughness data. The tests were carried out on highly cracked, single edge bend SE(B) specimens with a weld centerline notch covering I) shielded metal arc welding (SMAW) with and without a post weld heat treatment (PWHT) and ii) flux-cored arc welding (FCAW), which had been used in a previous study (Bianchi et al.2017). To serve as a benchmark toughness data set, additional fracture toughness measurements for the ASTM A572 Grade 50 baseplate material described in prior work by (V.S. Barbosa, C. Ruggieri, 2018) were included in the analysis. The dependency of cleavage fracture toughness on temperature in the DBT area for the investigated materials was determined using a statistical analysis based on the Master Curve technique on fracture toughness data received from testing the weld specimens. The test welds were also subjected to traditional Charpy-V notch impact testing to define their ductile-to-brittle transition and to correlate the CVN energy with fracture toughness.

Verification research findings of the correlation between CVN energy and fracture toughness for tested weldments fabricated by the SMAW and FCAW processes may provide nonconservative integrity assessment for imperfect structural parts because the calculated toughness value is higher than the experimentally tested values. On the other hand, using an alternative comparison expression in which T0 is clearly taken as the Charpy transition temperatures corresponding to 41J energy, the correlation between CVN energy and fracture toughness produces predicted toughness values that are significantly better than the

measured data values. Overall, the current study adds to the body of experimental evidence that supports the established correlations between fracture toughness with charpy impact energy when paired with other studies.
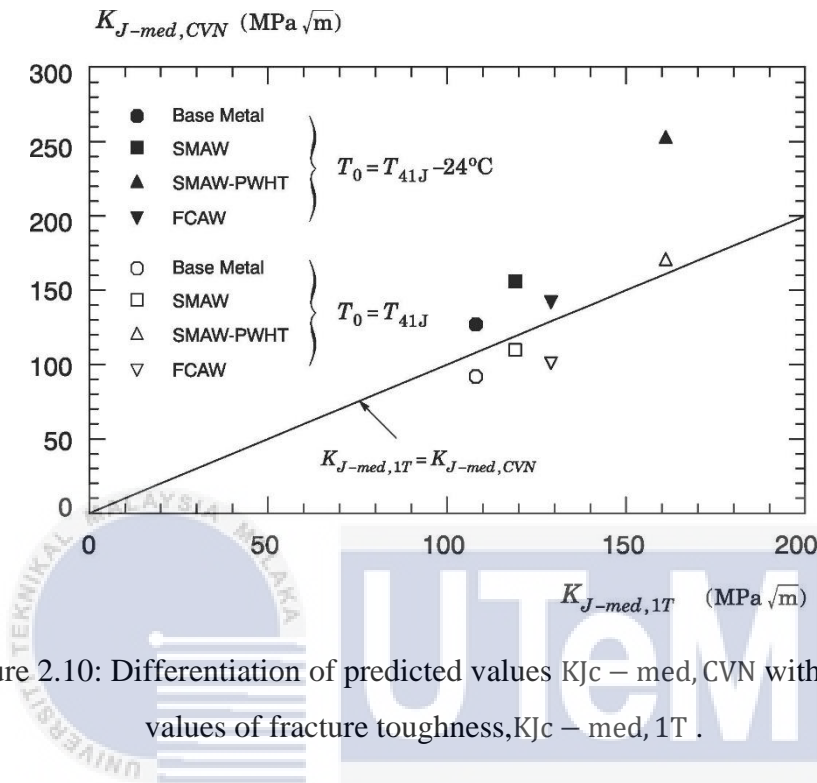
Figure 2.10: Differentiation of predicted values $KJc - med, CVN$ with experimental values of fracture toughness, $KJc - med, 1T$.

More addition research (Kunigita et al., 2020) [23], the findings of Charpy impact testing for a variety of simulated heat-affected zone (HAZ) samples with various chemical compositions and temperature cycles are presented in this work. The intended microstructure was coarse-grained, with upper bainite and martensite-austenite (MA) elements predominating. Microstructural characteristics were examined, including MA and grain boundary (GB) ferrite volume percentages, as well as statistical distributions of MA particle thickness, lath width, and GB ferrite thickness. All of this information was loaded into the computer model that was provided in Figure below to anticipate the Charpy impact absorbed energy transition behavior. The projected findings matched the experimental results rather well. The current model does not use data from different specimens; instead, the Charpy absorbed energy and scatter can be estimated solely from microstructural characteristics and

34

tensile properties. The Charpy absorbed energy of samples M1, M3, and M10 is shown in the image. As the cooling rate increased, the regression line for absorbed energy (dotted line) changed to a lower temperature, suggesting increasing toughness.
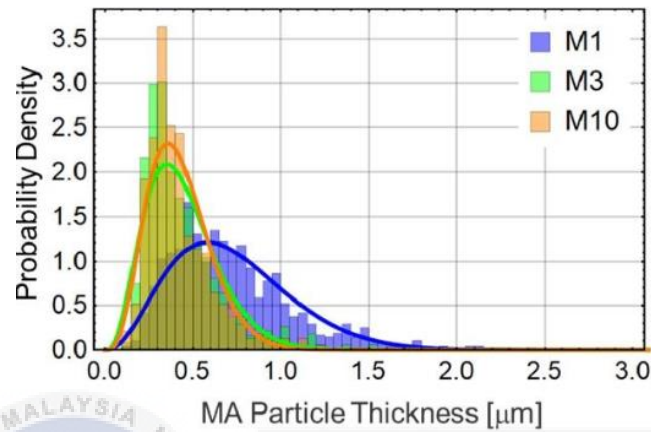
Figure 2.11:Statistical distributions of the microstructural parameters for the simulated HAZ for samples M1, M3 and M10 (Kunigita et al., 2020) [23].
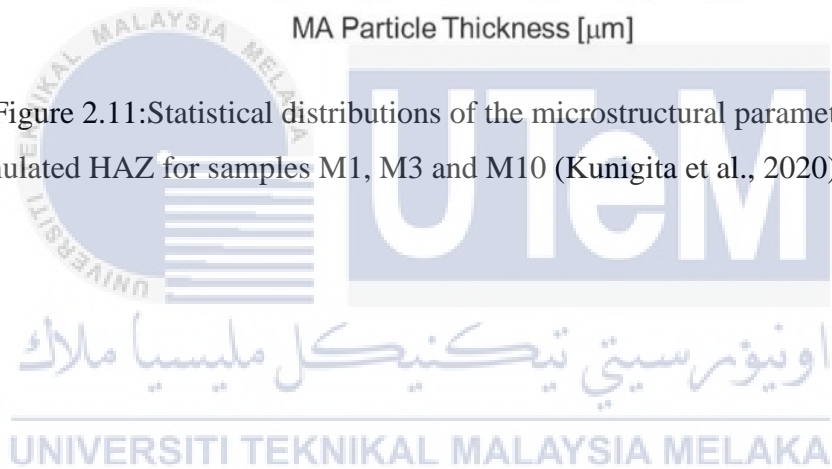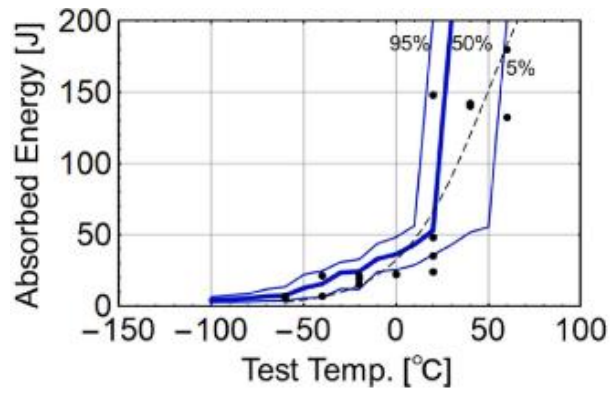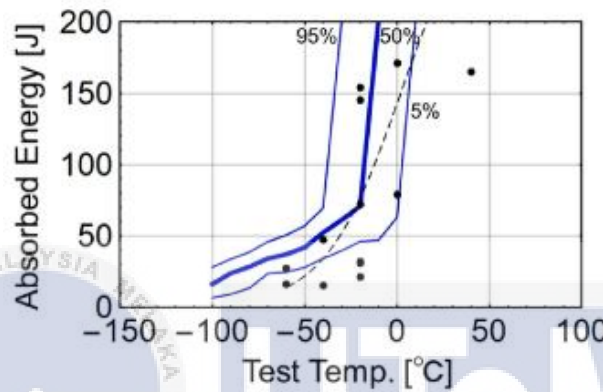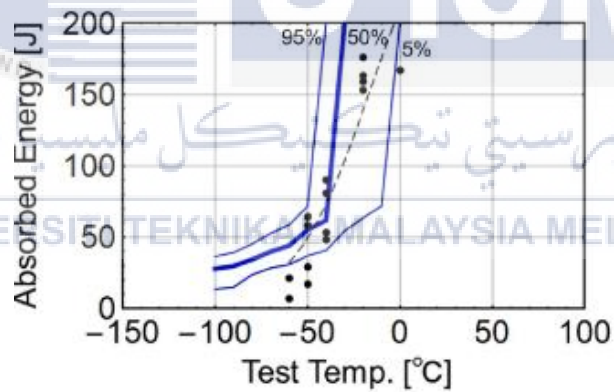
Figure 2.12:Charpy absorbed energy transition curves for the simulated HAZ, experimental and calculated, for samples M1, M3 and M10 (Kunigita et al., 2020) [23].

2.3   Steel in Automotive Industry

Since the 1920s, steel has been a frontrunner in automotive applications. Steel is currently the most common material used in body and chassis structures. It serves as the vehicle's foundation. Steel now accounts for around 65 percent of the weight of automobiles.

It has a variety of functions in today's cars. It protects occupants, gives a pleasant driving experience, reacts to road loads, provides comforts, and connects to other vehicle components.

Before being certified, materials used in the automotive sector must meet a number of requirements. Some of the criteria are the outcome of environmental and safety regulations and legislation, while others are the demands of automotive users. Different aspects frequently conflict, and a great automotive design can only be achieved through an optimum and balanced solution. Steel is utilized by automakers since it is the toughest and also most cost-effective suitable material for the job, and also can be fabricated in variety of ways to meet collision safety and vehicle performance requirements.
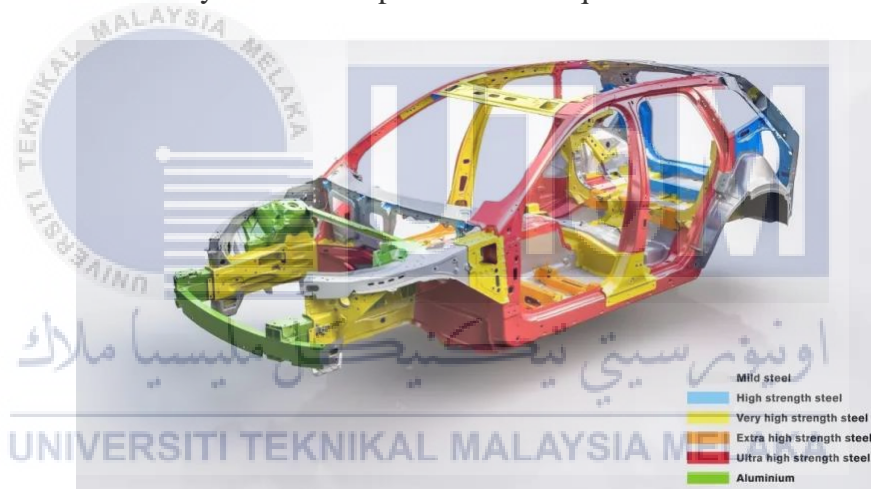
Figure 2.13:Image of different material on different parts of the automobile.

2.3.1 Mild Steel

Mild steel is an iron and carbon-based ferrous metal. It's a low-cost material with characteristics that make it suited for a wide range of engineering applications. Because of its high iron content, low carbon mild steel has good magnetic characteristics and is hence classified as ferromagnetic. Mild steel has a minimum carbon concentration of 0.16 percent and a maximum carbon content of 0.29 percent, with a melting point of 1450°C to 1520°C. Because of its high melting temperature, mild steel becomes more ductile when heated,

making it ideal for forging, cutting, drilling, welding, and fabrication. Mild steels typically have only one microstructure, ferrite (Black et al., 2013) [17].

The maximum tensile strength of these steels is 280 N/sq mm, and they are relatively easy to produce. The density of mild steel is approximately 7.85 g/cm3 (7850 kg/m3 or 0.284 lb/in3) and the Young's modulus is 200 GPa (29,000 ksi). Mild steels used to be the most common material in automobile bodies, but they're now only used for stiffness-related components and cosmetic sections that require a lot of bending and drawing. There are two main material types in this group, Mild steels (also known as low carbon or plain carbon steels), which have very little alloying element, and interstitial free (IF) steels, which have ultralow carbon and even lower strength but higher formability (Sarna, 2015) [16].

2.3.2　High Strength Steels (HSS)

Solid-solution hardening is the primary strengthening mechanism in conventional HSS. The chemistry and manufacturing of bake hardening (BH) steels are designed to remove carbon from solution during the paint baking cycle. The steel is made softer and more formable for the press shop in this manner, but it gains strength when it is put into service. Carbon manganese steels are solid solutions of mild steel that have been reinforced by the addition of manganese alloy. Carbon manganese steels containing a micro alloying element such as titanium, vanadium, or niobium are known as high strength low alloy (HSLA) steels. Despite having a tensile strength of up to 800 N/sq mm, these steels can still be press molded (Sarna, 2015) [16].

Table 2.1:SAE HSLA grade mechanical properties.

SAE HSLA steel grade mechanical properties[10]

Grade	Form	Yield strength (min) [psi (MPa)]	Ultimate tensile strength (min) [psi (MPa)]
942X	Plates, shapes & bars up to 4 in.	42,000 (290)	60,000 (414)
945A, C	Sheet & strip	45,000 (310)	60,000 (414)
	Plates, shapes & bars:		
	0–0.5 in.	45,000 (310)	65,000 (448)
	0.5–1.5 in.	42,000 (290)	62,000 (427)
	1.5–3 in.	40,000 (276)	62,000 (427)
945X	Sheet, strip, plates, shapes & bars up to 1.5 in.	45,000 (310)	60,000 (414)
950A, B, C, D	Sheet & strip	50,000 (345)	70,000 (483)
	Plates, shapes & bars:		
	0–0.5 in.	50,000 (345)	70,000 (483)
	0.5–1.5 in.	45,000 (310)	67,000 (462)
	1.5–3 in.	42,000 (290)	63,000 (434)
950X	Sheet, strip, plates, shapes & bars up to 1.5 in.	50,000 (345)	65,000 (448)
955X	Sheet, strip, plates, shapes & bars up to 1.5 in.	55,000 (379)	70,000 (483)
960X	Sheet, strip, plates, shapes & bars up to 1.5 in.	60,000 (414)	75,000 (517)
965X	Sheet, strip, plates, shapes & bars up to 0.75 in.	65,000 (448)	80,000 (552)
970X	Sheet, strip, plates, shapes & bars up to 0.75 in.	70,000 (483)	85,000 (586)
980X	Sheet, strip & plates up to 0.375 in.	80,000 (552)	95,000 (655)

2.3.3   Advanced High Strength Steels (AHSS)

Advanced High-Strength Steels (AHSS) are a necessity for a new generation of steel with high strength and formability at a reasonable cost. The third generation AHSS. According to the study (Sarna, 2015) [16] states that AHSS have been developed recently but only two types of these steels are under production currently. These are 'quenching and partitioning steel (Q&P steel) and TRIP aided bainitic ferrite steel (TBF steel).

Carbon, manganese, silicon, nickel, and molybdenum alloying elements are included in the Q&P steel grade. Alloying components can be as high as 4% depending on the strength level. It has been proved that Q&P steel with a strength of 1180 N/sq mm may be cold formed into a B-pillar reinforcement. When compared to DP steel of the same strength, Q&P steel is more formable and less prone to edge cracking. Q&P steels have been used for A- and B-pillar reinforcements by a number of automakers.

TBF steel is a low-alloy steel that may be made using existing heat treatment equipment. Stable maintained austenite is a fundamental component. TBF steels have been created with strengths ranging from 980 N/sq mm to 1470 N/sq mm. In some car models,

TBF steel with a strength of 1180 N/sq mm is utilized in the A- and B-pillars, as well as on the rocker reinforcements. TBF steels currently account for 4% of the white body in various variants. In the near future, some automakers intend to increase the use of cold formed, ultra-high strength steels by up to 25%.

2.4   Types of Welds

Welding is a method of combining materials called fabrication, primarily steel and thermoplastics, by fusing them together as one and letting them to rest, causing fusion.Welding, unlike relatively low-temperature processes such as brazing and soldering, doesn't really melt its base metal. The filler material is frequently added to the joint in addition to melting the base metal to create a pool of molten metal (the weld pool) that chills to create a joint which can be stronger and tougher metal based on the weld pattern (butt, total penetration, fillet, etc.). To make a weld, pressure can be employed alone or in association with heat. Welding additionally needs the employment of a shield to protect the filler material or molten metals from contaminate or oxidizing. Welding can be done with a gentle heat (chemical), an electrical arc (electrical), a laser, an electromagnetic wave, friction, and ultrasonic, among many other sources of energy. Welding could be done everywhere, including in the outdoors, under water, and even in space. Welding has a number of dangers, including burns, electrocution, vision impairment, inhalation of hazardous chemicals and gases, and exposure to severe UV radiation. There are three mainly types of welding, which is MIG or named as Gas Metal Arc Welding (GMAW), TIG or known as Gas Tungsten Arc Welding (GTAW) and Stick, which known as Shielded Metal Arc Welding (SMAW) (Cary, 2011) and (Weman, 2012) [19-20].

2.4.1 Sheild Metal Arc Welding (SMAW)

With this type of welding, the welder performs a manual stick welding process. The stick creates an arc here between stick and the metals to be linked by using an electric current. The open V-Groove is extensively used to weld iron, steel, and mild steel pipe in the building of steel structures and in industrial fabrication. Welders must be able to weld to the level where their output can survive a destructive bend test. Shielded metal arc welding is frequently used to connect carbon steel, alloy steels, stainless, ductile iron, and cast steel, but it can also be used to join nickel and copper. It is almost never used on aluminum (Lincoln Technical Institute,2021) [21].
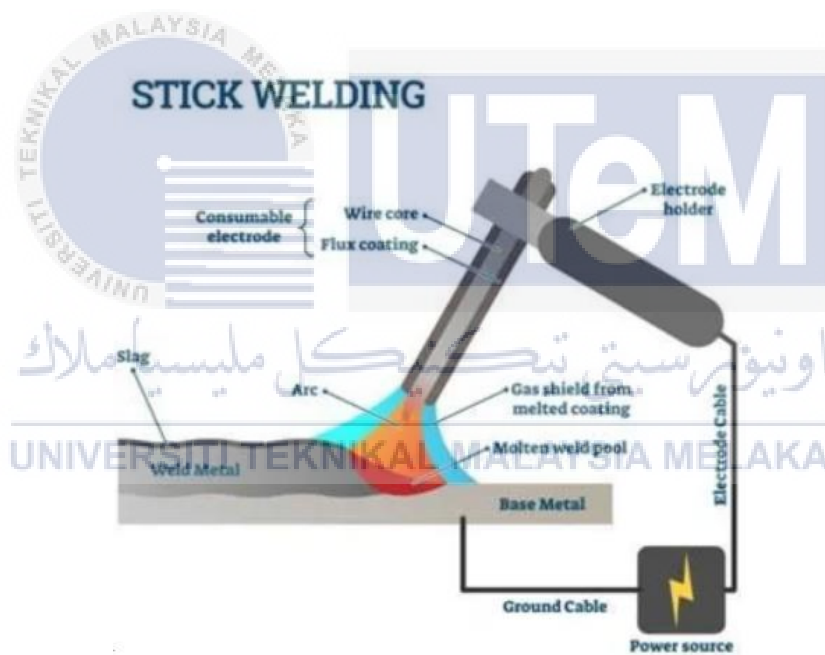
Figure 2.14:Configuration of SMAW process.

2.4.2 Gas Tungsten Arc Welding (GTAW/TIG)

Welding large chunks of stainless steel and non-ferrous metals together is the most prevalent application for this method. That is an arc-welding method that employs a constant consumable tungsten electrode to make the weld. Compared to MIG, Stick, or Flux Cored Arc Welding, this method takes a lengthy time. Because the melting points of nonferrous

41

metals vary greatly, attention must be taken while determining the composition of the base metal. Both Stainless Steel and Steel contain iron; nevertheless, to be classified as Stainless Steel, the metal must contain at least 11% Chromium. Carbon steel melts at temperatures ranging from 2,600 to 2,800 degrees Fahrenheit. The presence of 11% chromium in stainless steel limits the temperature range to 2,750+/- degrees F. Nothing, however, demonstrates welding talents more than the complex ability to TIG weld aluminum. To create a smooth, spectacular weld, you need a steady hand, a skilled eye, and an artistic touch (Lincoln Technical Institute,2021) [21].
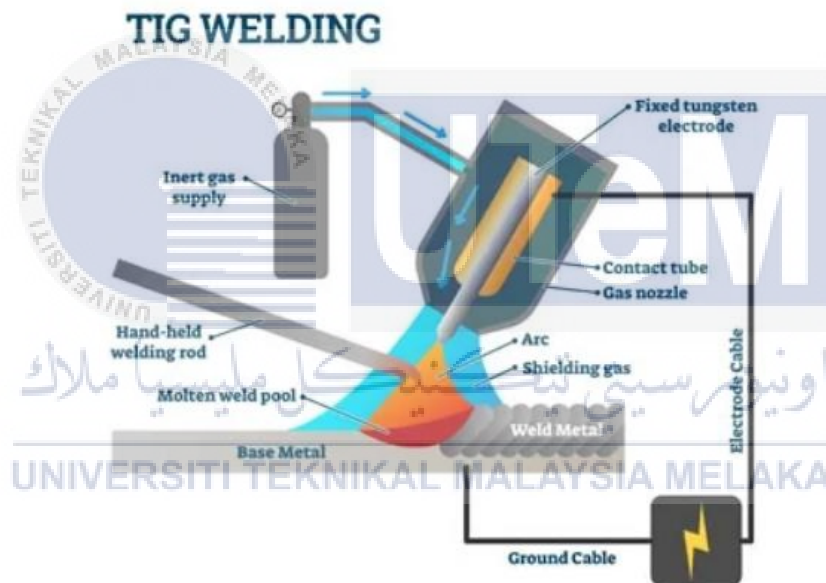
Figure 2.15:Configuration of TIG process.

2.4.3   Gas Metal Arc Welding (GMAW/MIG)

This type of welding process is also known as Metal Inert Gas welding (MIG). By flowing a shielding gas along on the wire electrode, it heats melts the two metals to be joined. The most widely used industrial welding process, which includes plate and large bore pipe, necessitates a consistent voltage and direct-current power supply. (Lincoln Technical Institute,2021) [21].
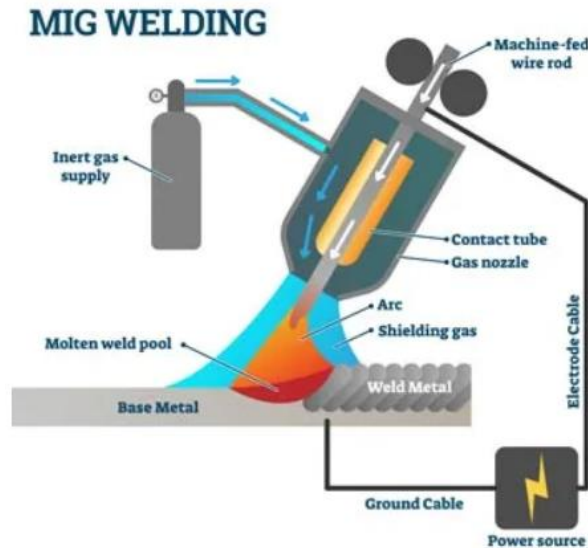
Figure 2.16:Configuration of MIG process.

In MIG welding, a shielding gas is commonly used to assist protect the weld joint from contamination. Inert gas metal welding does not use shielding, as the name implies. MIG welding is impossible without hydrogen shielding. The MIG welding method is another reason for the shielding gas choking the weld. This makes it easier to operate with welding, fusion arcs, and fusion wire in a clean environment." Argon, carbon dioxide, and helium are the three most common shielding gases used in MIG welding.

Based on research (Madavi et al., 2022) [29]. On Metal Inert Gas welding procedures, the influence of activating flux on tensile strength of Fe410 mild steel is investigated, and the optimal value is determined using the L9 array. The procedure is to join two dissimilar metals, Stainless Steel 304 and mild steel, in accordance with the joining of metals SA-508 grade III and SS-304 LN, by performing experiments and altering process parameters to develop good quality welds. The purpose of the research is to look at the microstructural evaluation of successful weld metal. On the result, it is shown that different parameters such as filler wire, feed rate, current supply and welding technique do give a various impact on the microstructural properties of the mild steel

43

CHAPTER 3

METHODOLOGY

3.1   Introduction

The study of the procedures utilized in an area of study is referred to as methodology. It is a methodical approach to completing tasks and therefore is defined as the set of methods, techniques, tools, and document aids that aid in the explanation and demonstration of the development phase (Pressman, 2001). The research methodology's objective is to give an overview of the methodologies that were used in this study. This chapter explains various methodologies that were used in gathering data and analysis which are relevant to the research. It also provides description, explanation, and planning details of the project. These includes, characteristics of selection material, creating specimens, identifying the parameter of specimen, identifying parameters of welding, identifying the parameters and process of EDM wire cutting, the operations of Charpy impact test and the application of strain gauge.

3.2   Flowchart

A process flowchart is a graphical representation that shows the sequential stages of a procedure as well as the choices that must be taken for the process to work. In the chart/visual representation, each step is represented by a shape. A shape represents this stage. To indicate the flow and direction of the process, lines and arrows connect these forms. This study begins with the material selection and specimen preparation before experimental work on instrumented Charpy and tensile test were conducted. Data of energy absorbed and impact strain signal from Charpy test are collected to analysed in terms of energy absorbtion (J) and strain-time (ε-t) graph. While data from tensile test is analysed to identify the mechanical properties

44

such as young's modulus, yield, ultimate and fracture strength of each material. Tensile data is used to observe the material behaviour based on the stress-strain curve.
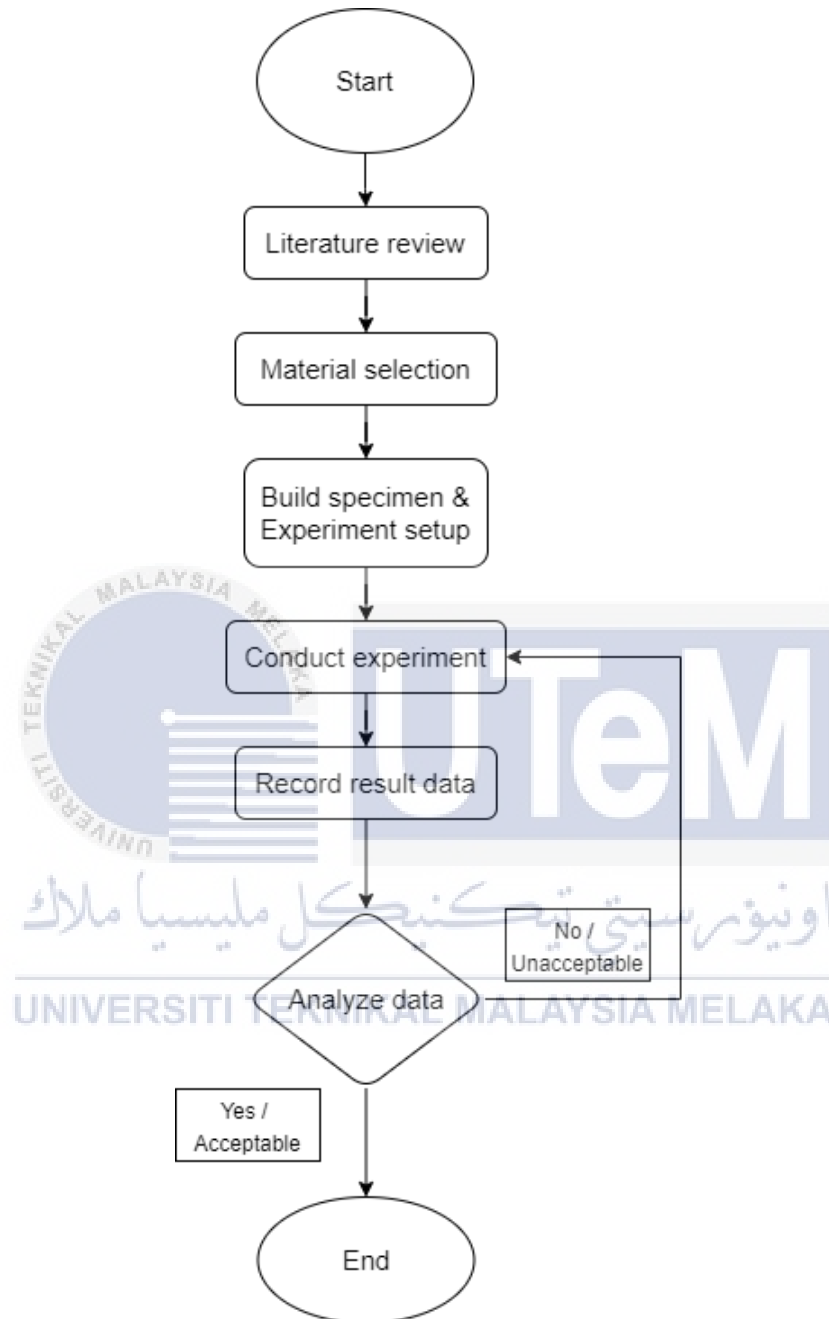
Figure 3.1: Flow chart presents the activities involved in research study.

3.3 Material Selection

In this study, both for the welded and unwelded material specimens were made from mild steel material which has great magnetic properties and is hence classified as ferromagnetic. Mild steel has a minimum carbon concentration of 0.16 percent and a maximum carbon content of 0.29 percent, with a melting point of 1450°C to 1520°C. The maximum tensile strength of the steels is 280 N/sq mm, The density of mild steel is approximately 7.85 g/cm3 (7850 kg/m3 or 0.284 lb/in3) and the Young's modulus is 200 GPa (29,000 ksi). In addition, materials of specimen were chosen based on material that is often used in production of common material in automobile bodies, which is used for stiffness-related components and cosmetic sections that require a lot of bending and drawing. In this case, the material should have some criteria such as corrosion resistance, durable, easy to obtained and low cost.

3.4 Experiment Preparation and Setup

This project must have the prerequisite tools, materials, software, and appropriate machines to meet the project's objectives. The mentioned items are as below: -

1. Tensile specimen
2. Welded material specimen
3. Unwelded material specimen
4. Strain gauge sensor

3.4.1 Tensile Specimen

Dog bone tensile test samples are primarily used in tensile tests. The sample has a gauge portion in the middle and a shoulder at either end. When the sample is loaded with a tensile force, the shoulders are broader than the gauge section, causing a stress concentration in the center. The dog bone shape tensile specimen is made with same material as the unwelded and

welded material specimen, it is to provide base information or reference to correlate with the result of the test
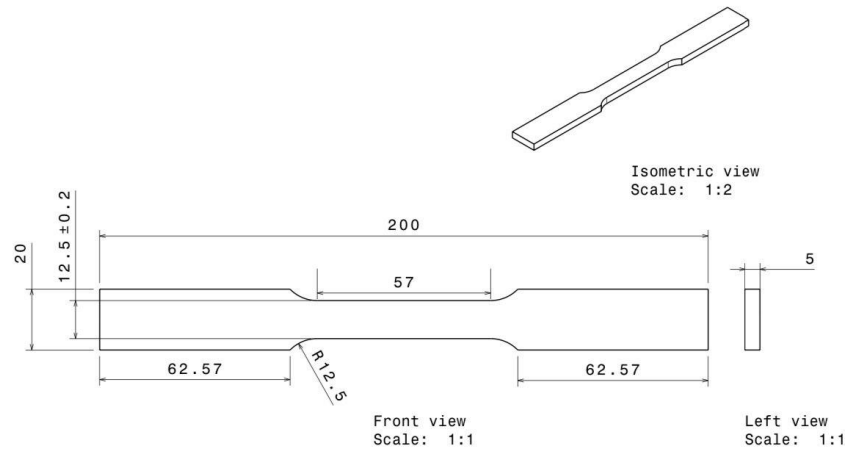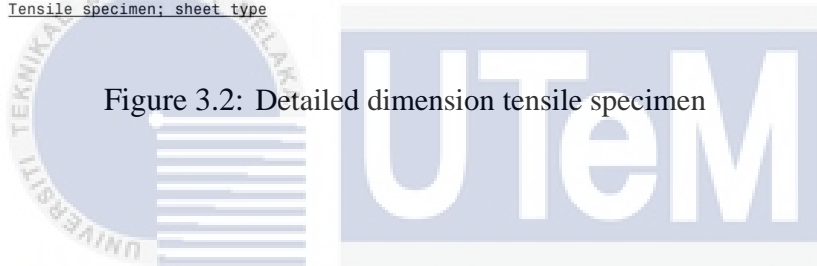
Figure 3.2: Detailed dimension tensile specimen

The dog bone specimen has a width of twenty millimeters (20mm), length of two hundred millimeters (200mm) and thickness of five millimeters (5mm). The reduced section is fifty-seven millimeters (57mm) long, width of twelve point five millimeters (12.5mm) with tolerance of zero point two (±0.2) and grip section of sixty-two point five seven millimeters long (62.57mm).

3.4.1.1 Tensile Specimen Making Process

In order to create the tensile specimen from the material, a certain process must be done to produce an accurate and fine specimen. These steps including parting the material, machining and finishing. Figure 2.3 shows the flow procedure of making tensile specimen. Table below explains the procedure used to make the tensile specimen:
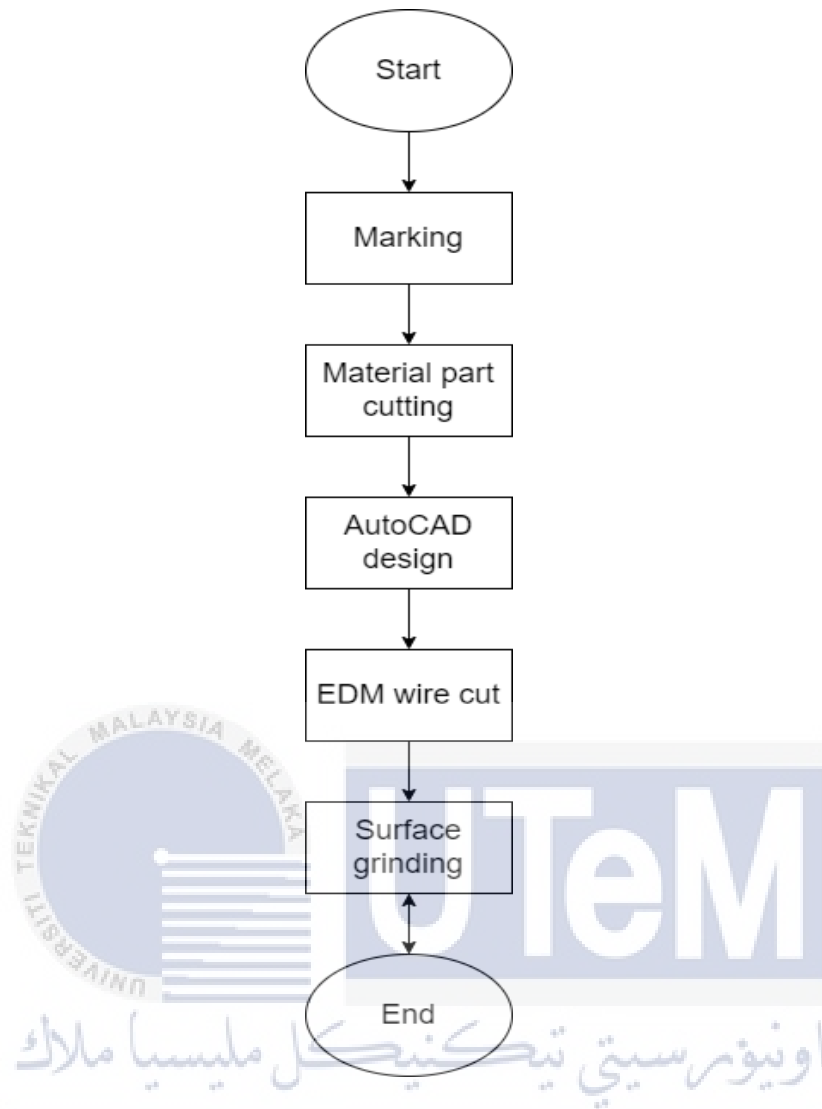
Figure 3.3: Tensile specimen basic procedure

Table 3.1: Tensile Specimen Making Process

No.	Process	Description
1.		- Mark down the cutting line on steel using ruler and scriber, the length should be 200mm (±0.2)
2.		- Cut the steel using bench saw machine. Make sure the cutting line behind the cutting mark.
3.		- Design the specimen using AutoCAD software according to the diameter required. (For EDM wire cut purpose)
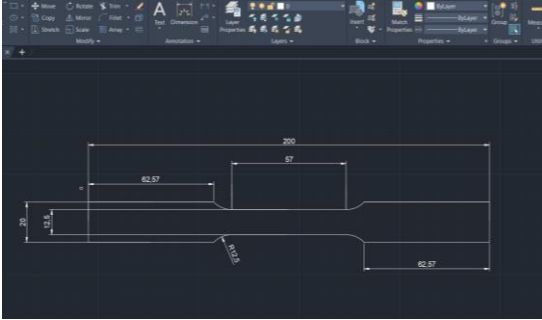
4.		- The material is processed with an EDM wire cutter. The machine makes cuts based on the AutoCAD data.
5.		- The specimen is then grinded until it reaches the accurate thickness and better surface finishing.

3.4.2 Welded Material Specimen

The Charpy Impact Test determines how much energy a standard notched specimen absorbs while breaking under impact. The Charpy Impact Test is still used to measure the notch sensitivity and impact toughness of engineered materials as an economical quality control procedure. The welded Charpy Impact Test specimen is a metal bar that are weld together with a certain parameter to have fillers filled in the middle of the specimen shaping like a trapezoid angle.
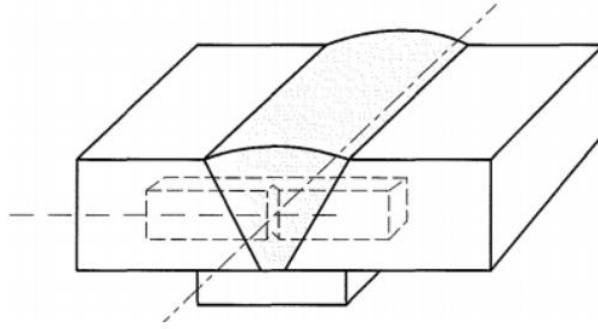
Figure 3.4: Configuration of welded specimen

The welded metal bar which has a length of one hundred and fifty millimeters long (150mm), width of seventy millimeters (70mm), and thickness of fifteen millimeters on each side. To create a slope for welding, each side of the bar has a 30-degree angle of slope and the metal bars were welded together with a 2mm space between them. The needed specimen is located at the center of the weld specimen where the weld filler must be perpendicular with the v notch marking on the specimen.

3.4.2.1 Welded Material Making Process

A certain technique must be followed in order to get an accurate and fine welded specimen from the material. These steps include material parting, machining, welding and finishing. The flow diagram for manufacturing weld material specimens is shown in Figure 2.3. Table 3.3 explains the procedure used to make the welded specimen:

51
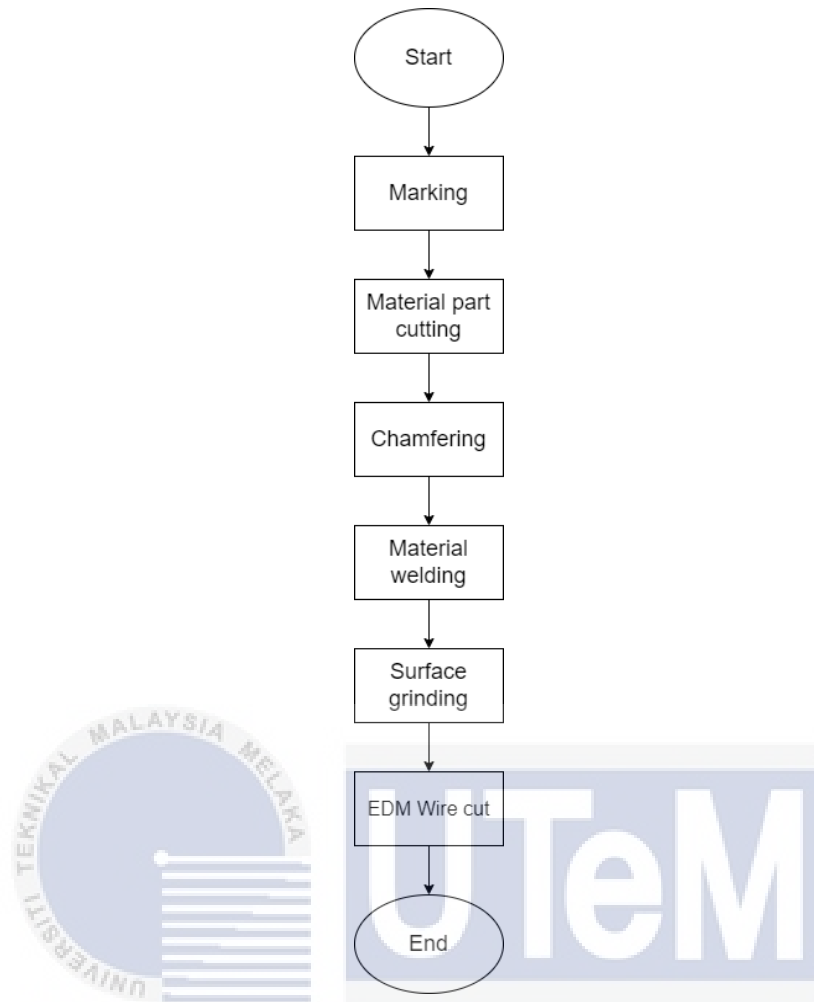
Figure 3.5: Welded specimen basic procedure

Table 3.2: Welded Material Making Process

No.	Process	Description
1.		- Mark down the cutting line on steel using ruler and scriber, the length should be 150mm.

2.		- Cut the steel using bench saw machine. Make sure the cutting line behind the cutting mark.
3.		- mark the 30-degree angle on each side of the metal bar with protractor and mark down using scriber. - Make sure to leave 1mm gap range from below for welding process purpose.
4.		- Mill the edge of the metal bar until it reaches a required angle. (Cut feed is 0.5mm on each run).

5.		- Weld the metal together and use weld filler to cover the 60-degree angle grove.
6.		- Grind the weld material to get better surface and required thickness.
		- Cut the weld material by section to produce precise dimension weld specimen.

3.4.2.2 SMAW Weld Process

Welding of the mild steel plate was performed using the shielded metal arc welding (SMAW) process in the 1G (flat) position with a single V-groove configuration shown in figure below.
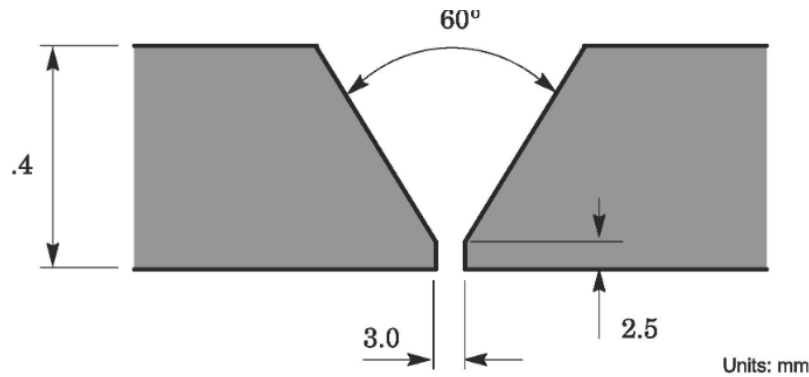
Figure 3.6: Schematic of the single V-groove design used to fabricate the test weld joint.
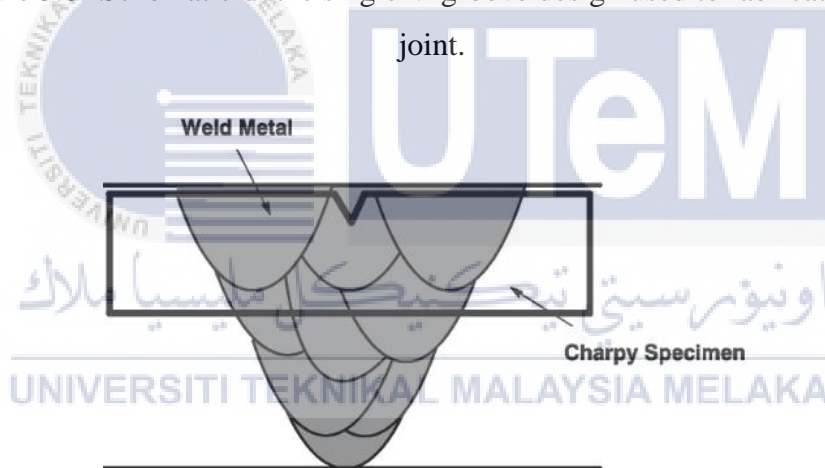
Figure 3.7: Positioning of the Charpy specimen and its notch at the weld centerline region.

Welding sequence or welding pass is an important criterion of the welding process that determines weld quality. Welding passes are simply the flow of the welding process or the order in which welding should be performed. Welding passes are the sequences of welding. A standard welding procedure consists of four passes. There are four of them: Root Pass, Hot Pass, Fill up Pass, and Capping. The main weld parameters used for preparation

55

of the test weld using the SMAW process are by using arc rod filler metal MS6013 with diameter of 0.4mm. The following pass parameters of weld is as the table below.

Table 3.3: Pass parameters of weld

Type of passes	Current setting (A)	Number of passes
Root Pass (Penetration pass)	85	1
Hot Pass	120	1
Fill Up Pass	100	3
Capping	95	3

3.4.3 Unweld Material Specimen

Charpy specimen was designed according to standard stated in American Standard for Testing and Material (ASTM) E23 where the size is 55 mm (length, l), 10 mm (height, h) and 10 mm (width, w). Specimen has a v-notch of 45° with 0.25 mm of root radius and depth of 2 mm. Detailed dimension of the specimen is shown in Figure 3.6 below. Since thickness (or width) of specimen is one of the parameters in this study, sub-sized specimen with thickness of 5 mm and 7.5 mm must also be prepared. Before the Charpy test is conducted, all the test pieces must be marked by using Vernier calliper at both end of the test piece with 7.5 mm as shown in Figure 3.7. The marked acts as a reference point when placed on anvils before the hammer of machine is released.
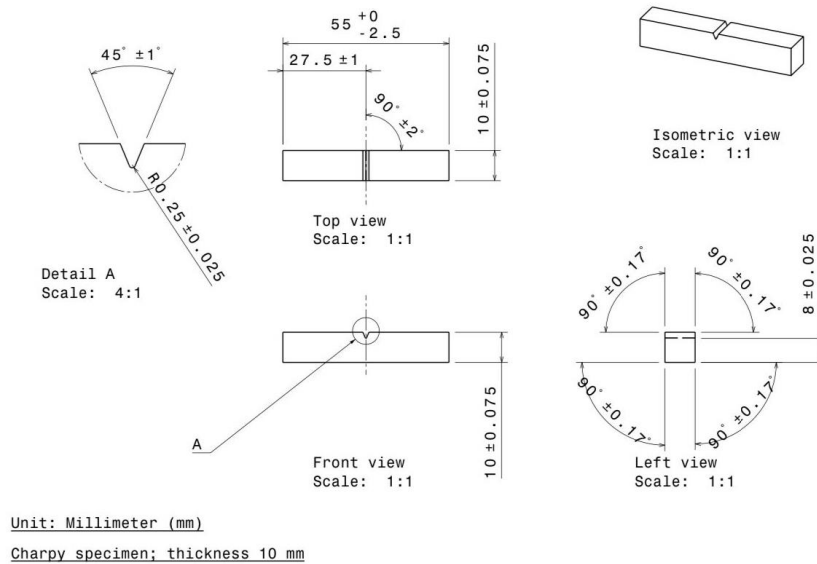
Figure 3.8: Detailed dimension Charpy specimen.

Figure 3.9: Marked Charpy specimen

3.4.3.1 Unwelded Material Making Process

A certain technique must be followed in order to get an accurate and fine tensile specimen from the material. Partitioning the material, machining, and finishing are some of these procedures. The method of developing a tensile specimen is depicted in Figure 2.3. Table 3.5 below explains the procedure used to make the unwelded specimen:

57
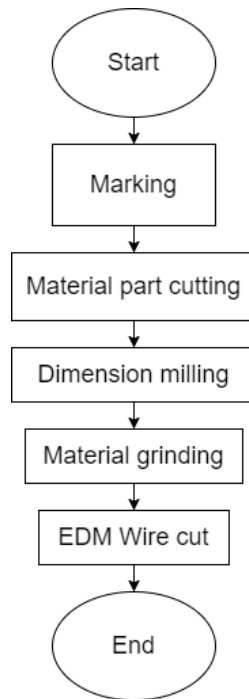
Figure 3.10: Unwelded specimen basic procedure

Table 3.4: Unwelded Material Making Process

No.	Process	Description
1.		- Mark down the cutting line on steel using ruler and scriber, the length should be 150mm.

| 2. | | - Cut the steel using bench saw machine. Make sure the cutting line behind the cutting mark. |
| 3. | | - Marking down the needed size for the specimen (10mm,7.5mm, and 0.5mm) |

4.		- Milling down the surface of the steel to get the exact height, and length of the specimen. (55mmx10mmx150mm)
6.		- Grind the material to get better surface and accurate thickness.
		- Creating V-notch on the plate and cut the material by section to produce precise dimension specimen.

3.4.4 Strain Gauge Sensor

In order to capture the dynamic response of the strain signal from the Charpy impact test, a strain gauge is installed on the striker of the Charpy machine, which is connected to a high frequency data gathering system. Figure 3.9 depicts the basic installation techniques for the strain gauge. The installation must be done carefully and accurately.
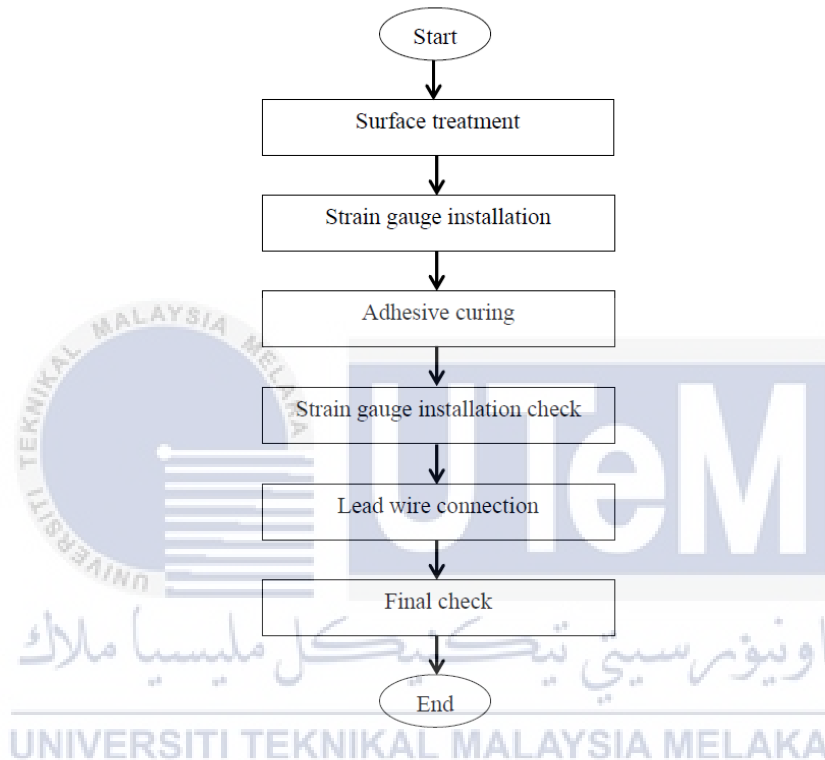
Figure 3.11:Strain gauge installation basic procedures

Cleaning the installation area of the striker surface with sandpaper to remove extraneous material such as grease or dirt was the first step in installing the strain gauge. The surface is then wiped down with a cloth. As a reference for installation, the strain gauge mounting location is marked with a pencil on the striker surface. A strip of cellophane tape is stuck under the gauge wire led to prevent direct contact of the wire lead with the striker, preventing a short circuit. Cellophane tape is wrapped over the wire lead to preserve it and keep it from shifting. The smooth side of the strain gauge is then connected to the striker surface with polyethylene sheet before the strain gauge cement glue is applied. After

61

dropping glue on the strain gauge, thumb pressure is applied to the polyethylene sheet. To prevent the strain gauge from being pulled out during the impact test, the adhesive must be completely dry before the polyethylene is removed.

3.5 Charpy Impact Test

Charpy test is conducted by using Charpy impact tester Model JBW-500 Computer Pendulum Impact Testing Machine and carried out by referring to American Society for Testing and Materials E23 (ASTM E23) and International Organization for Standardization (ISO) 148-2. Charpy machine model specifications are as shown in the Figure.

II .Main Specifications

1. Impact energy: 250J, 500J
2. Impact velocity: 5.4m/s
3. Raised angle :150°
4. Effective weight pendulum 20-35 kg
5. Standard span: 40mm
6. Round angle of jaws: R1-1.5mm
7. Round angle of striking Edge: R2-2.5
8. Automatic lifting of pendulum hammer with motor and gear box
9. The release of pendulum through push button operation
10. The braking of pendulum is automatic through automatic clutch and torque limiter system
11. Two type of pendulum (big and small)and two scales reading enlarge the test range of energy
12. Fully cover with safety guard
13. Size of specimen: 10 x 10 x 55mm
14. Power supply: 3 phs, 380V, 50Hz, 180W

Figure 3.12:Charpy impact tester Model JBW-500 Computer Pendulum Impact Testing Machine specifications

Before running the impact test, the Charpy machine is calibrated to guarantee that the results are realistic and acceptable. Calibration of the Charpy machine is done by releasing the hammer where there is no specimen put on the anvils and obtaining a zero reading on the scale to prove that the machine is in good working order. After calibration on

the Charpy machine, the portable striker is removed from the hammer for strain gauge installation. After the strain gauge is inserted, the striker is reinstalled on the Charpy machine's hammer. The strain gauge is then connected to the gauge connection terminal, which is connected to the high acquisition system data, Somat eDAQ. The computer is linked to the eDAQ system to monitor the dynamic responses of the strain signal caused by the impact force. However, before the machine's latch is released, the data acquisition system (Somat eDAQ) software is configured, and calibration on the strain signal on the eDAQ software is performed for each test piece to minimise vibration and produce a smooth amplitude of the signal.

After setting up the eDAQ software, the Charpy specimen is placed on anvils and the reading scale of absorbed energy is set to zero before the hammer is released. Figure 3.6 depicts the configuration of the test specimen on the machine's anvils. Each sample was tested three times at varied parameters. Finally, energy absorbed and strain signal data were gathered and recorded. When the test piece jams in the machine, the results can be ignored and the machine thoroughly checked for any damage that could compromise its calibration. The quantity of energy absorbed shall not exceed 80% of the actual initial potential energy, according to ISO 148-2.
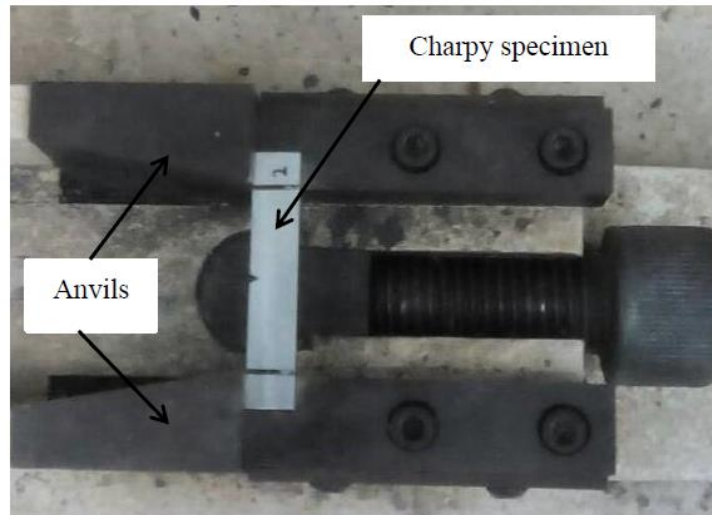
Figure 3.13:Configuration of specimen on anvils

3.6   Tensile Test

The most common mechanical testing to examine the mechanical performance of a material under an acting force is the tensile test. This test was used to discuss the material behavior based on the stress-strain curve, in addition to the ductile-brittle transition (DBT). Furthermore, the area under the stress-strain curve and the load-displacement graph are used to determine strain energy and energy absorbed under axial tension force, respectively. For tests employing the strain control method defined in ISO 6892, a Shimadzu Autograph AG-100 KNG Universal Testing Machine (Shimadzu Scientific Instruments, Kyoto, Japan) will be used. As indicated in Figure 3.11, the machine's capacity is 25 kN. The tensile test is carried out in accordance with ASTM E8 at room temperature with a crosshead speed of 2 mm/min. The loading rate was chosen since it was both within the speed range and sufficient and suitable for use during the tensile test. Each test component is tested three times. Following the tensile test, the obtained data is utilized to plot a stress-strain curve to determine Poison's ratio, young modulus, and material strength, which includes tensile, yield, and ultimate strength.

64

Figure 3.14:Shimadzu Autograph AG-100 KNG Universal Testing Machine

CHAPTER 4

RESULTS AND DISCUSSION

4.1   Introduction

This chapter presents and discuss the effects of different parameters which is type of materials and material thickness on the results of energy absorption and impact strain signal behaviors due to Charpy impact test. Findings from Charpy impact test was used to investigate the correlation of absorb energy between welded and unwelded (based) material. This chapter also analyze the study of impact signal between the welded and unwelded material. Hence, covers the study of material thickness effect on impact duration.

4.2   Charpy Impact Test

The findings of the experimental V-notch Charpy impact (CVN) test was presented in this section. The Charpy test yields data for energy absorbed and strain signal responses, which are both direct and indirect outcomes. Results of energy absorption are directly received from the Charpy machine's reading scale, whereas the behavior of the strain signal is determined by a strain gauge put on the striker machine. The effects of various parameters on the findings are described and supported in this subchapter along with all of the CVN results that were presented.

4.2.1   Absorb Energy of Welded and Unwelded Material

The specimen's absorb energy has been determined for every type and thickness by the impact test. Three tests are done on every material thickness and material type. The three data received from each party will be used to determine the data's average value. The

outcome displayed on the analogue scale is recorded directly and presented as Table 4.1, Table 4.2 Table 4.3 Table 4.4 Table 4.5 and Table 4.6.

Table 4.1 Absorb Energy of Unwelded specimens 10mm thickness
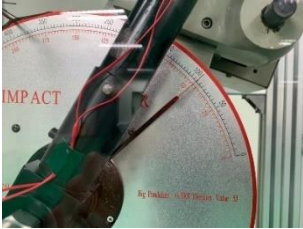
No.	Dimension	Scale Image	Value(J)
1.	10x10x55mm		90
2.	10x10x55mm		110
3.	10x10x55mm		125
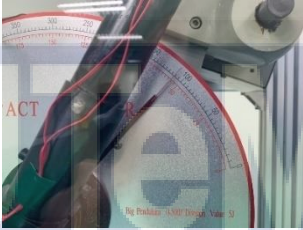
From the table 4.1 the receive value of absorb energy for a 10mm specimen, where the first test yields a minimum value of 90J, a second test yields a value of 110J, and the third test yields a maximum value of 125J.

Table 4.2 Absorb Energy of Unwelded specimens 7.5mm thickness

No.	Dimension	Result Image	Value(J)
1.	10x7.5x55mm		80
2.	10x7.5x55mm		82.5
3.	10x7.5x55mm		75

The receive value of absorb energy for a 7.5mm specimen is shown in Table 4.2, with the third test having a minimum value of 75J, the first test having an average value of 80J, and the second test having the highest value of 82.5J.

Table 4.3 Absorb Energy of Unwelded specimens 5mm thickness

No.	Dimension	Scale Image	Value(J)
1.	10x5x55mm		62.5
2.	10x5x55mm		62.5
3.	10x5x55mm		65

According to Table 4.3, the receive value of absorb energy for a 5mm unwelded specimen is 62.5J for the first and second tests, with the third test having the highest absorb energy value at 65J.

Table 4.4 Absorb Energy of Welded specimens 10mm thickness

No.	Dimension	Scale Image	Value(J)
1.	10x10x55mm		125
2.	10x10x55mm		130
3.	10x10x55mm		144

The receiving value of absorb energy for the 10mm welded specimen is shown in Table 4.4. The first test has the lowest energy value, 125J, the second test has a value of 130J, and the third test has the highest absorb energy value record, 144J.

Table 4.5 Absorb Energy of Welded specimens 7.5mm thickness

No.	Dimension	Scale Image	Value(J)
1.	10x7.5x55mm		85
2.	10x7.5x55mm		82
3.	10x7.5x55mm		80
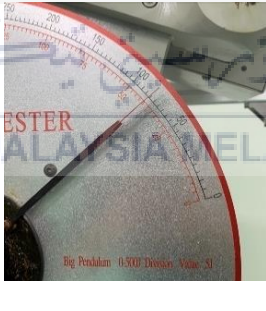
Table 4.5 shows the receiving value of absorb energy for the 7.5mm welded specimen. The energy value of the first test is 85J, followed by the values of the second and third tests, which are 82J and 80J, respectively.

Table 4.6 Absorb Energy of Welded specimens 7.5mm thickness

No.	Dimension	Scale Image	Value(J)
1.	10x5x55mm		50.
2.	10x5x55mm		45
3.	10x5x55mm		52.5

Table 4.6 shows the receiving value of absorb energy for the 5mm welded specimen. The energy value for the first test is 50J, the lowest value for the second test is 45J, and the highest absorb energy value ever recorded is 52.5J for the third test.

4.2.2 Impact Strain Signal of Welded and Unwelded Material.

The time and frequency domains of the strain signal were examined. The dynamic response of the strain signal from the Charpy impact test is read using a strain gauge, and the data is then sent to the SOMAT eDAQ system. Results of the impact strain signal were exported into the InField program in 'SIE' format. The impact time of the collected strain signal data is 3–4 seconds. Impact occurs in milliseconds (ms), hence the deformation of the strain signal is insufficient. The strain signal must therefore be chosen by enlarging the deform area where the impact time is optimal. The signal graph is then captured and exported to Excel, where it is extracted and combined with the other graphs into a category for straightforward discussion. Figures 4.1, 4.2, 4.3, 4.4, 4.5, and 4.6 combine the graph of the same material and thickness, each of which has undergone three tests. This will make it possible to compare the readings and provide the signal's average. The findings of the same material but with varying thickness are then analyzed using the chosen average signal, as shown in figures 4.7 and 4.8.

Figure 4.1 Unwelded specimens 10mm strain over time graph

The graph of the strain over time signal for unwelded specimens with a 10mm thickness may be seen in figure 4.1. The strain signal graphs from the first, second, and third runs are combined and stacked on top of one another. With the exception of the first run graph, whose impact duration is a slight bit shorter than the other two, the second and third test graphs generated nearly the same pattern. In terms of strain value, the second run has the biggest amplitude, which is approximately -350 (µℇ).

Figure 4.2 Unwelded specimens 7.5mm strain over time graph

The graph of strain over time signal for unwelded specimens with 7.5mm thickness is shown in figure 4.2. The strain signal graphs from the first, second, and third runs are combined and stacked on top of one another. With the exception of the third run graph, which has an impact period that is slightly shorter than the other two, the first and second test graphs showed patterns that were nearly identical. Regarding the strain value, the first run has the biggest amplitude, which is almost -250 (µℇ).

Figure 4.3 Unwelded specimens 5mm strain over time graph

Figure 4.3 displays a graph of the strain versus time signal for unwelded specimens with a thickness of 5 mm. The strain signal graphs from the first, second, and third runs are combined and stacked on top of one another. With the exception of the third run graph, which had an impact period slightly longer than the other two, the first and second test graphs showed patterns that were nearly identical. In terms of strain value, the third run has the largest amplitude, almost as low as -140 ($\mu\epsilon$). The third graph also differs from the first and second graphs in that the strain pattern starts to decrease at a point that is slightly lower than previous graphs—approximately -20 ($\mu\epsilon$).
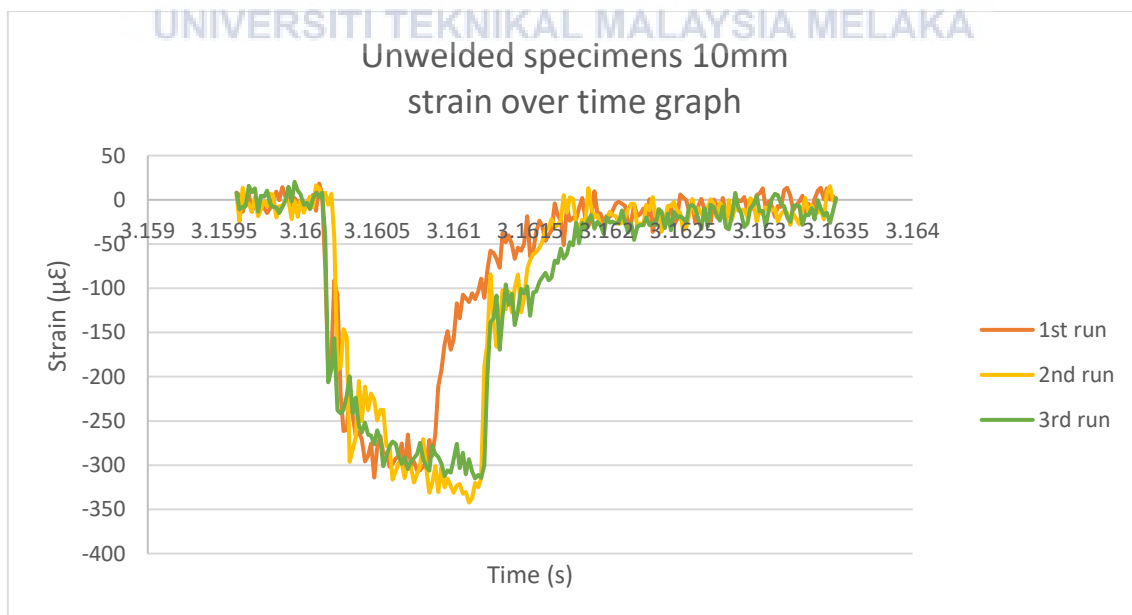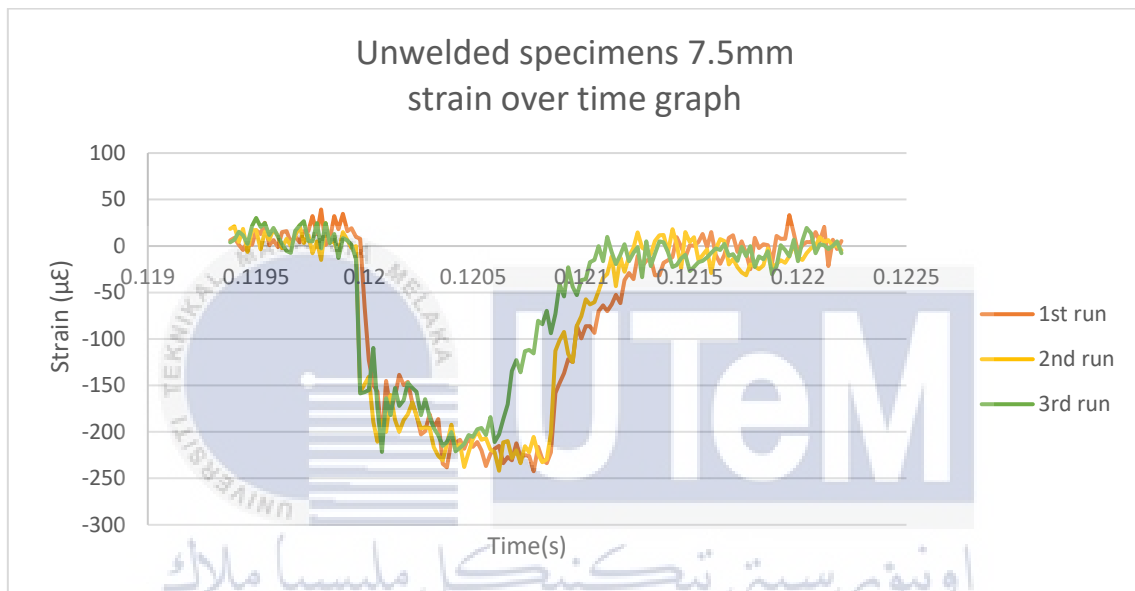
Figure 4.4 Welded specimens 10mm strain over time graph

The graph of the strain over time signal for welded specimens with a 10mm thickness may be seen in figure 4.4. The strain signal graphs from the first, second, and third runs are combined and stacked on top of one another. With the exception of the first run graph, whose impact duration is a little bit longer than the other two, the third and second test graphs showed nearly the same pattern. In terms of strain value, the second run has the biggest amplitude with a value close to -350 ($\mu\varepsilon$).
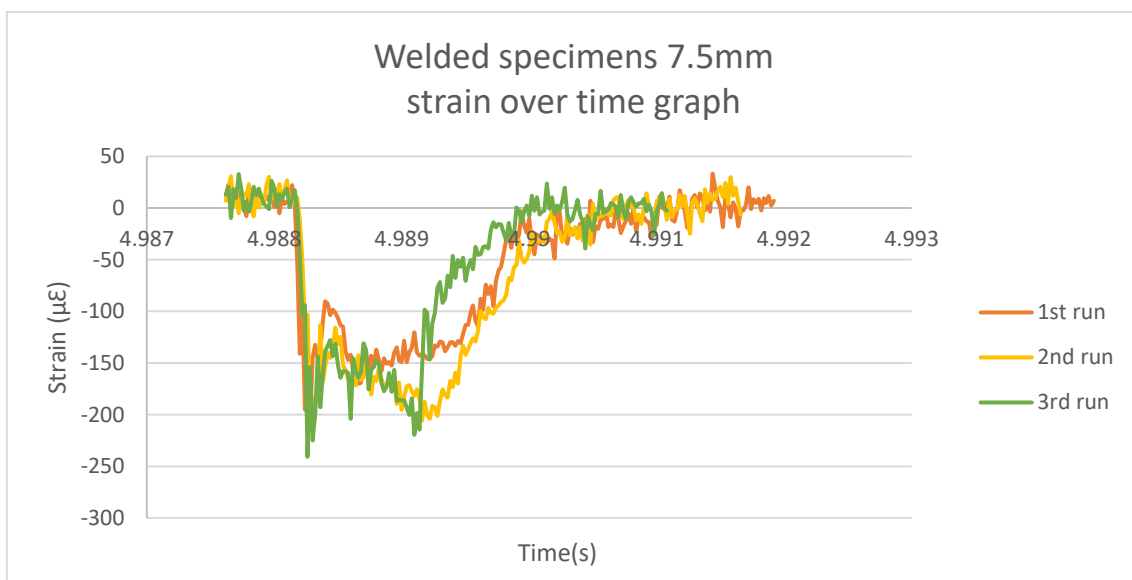
Figure 4.5 Welded specimens 7.5mm strain over time graph

76

A graph of the strain vs time signal for welded specimens with a 7.5mm thickness can be seen in figure 4.5. The strain signal graphs from the first, second, and third runs are combined and stacked on top of one another. This demonstrates that, with the exception of the second run graph, the third and first test graphs showed nearly the same pattern. Although the third graph's impact time is a little bit less than the other two, it has the biggest amplitude of strain, with a value that is about -250 ($\mu\mathcal{E}$).
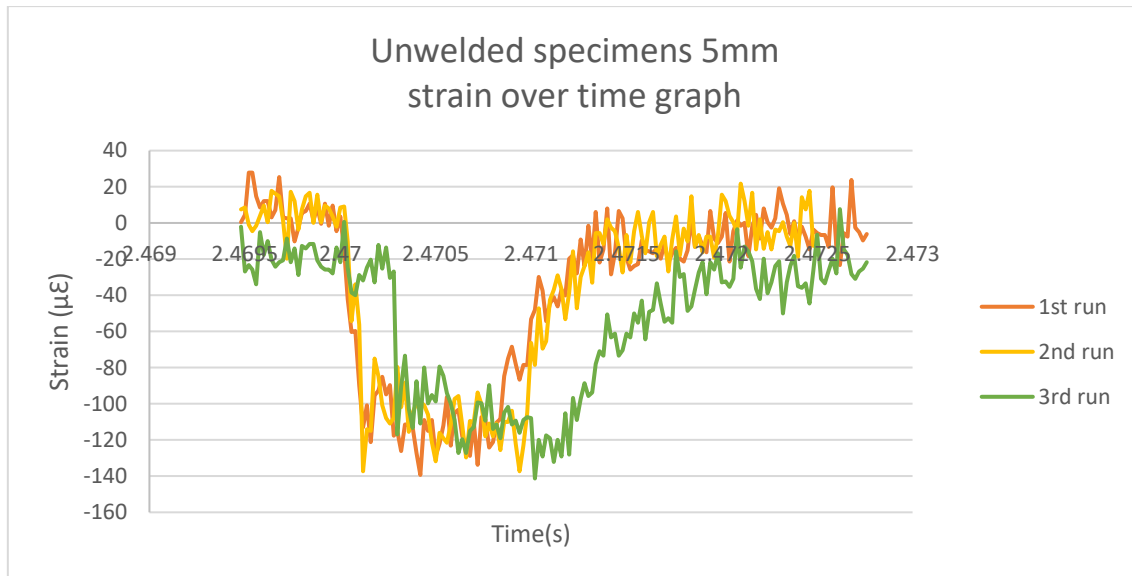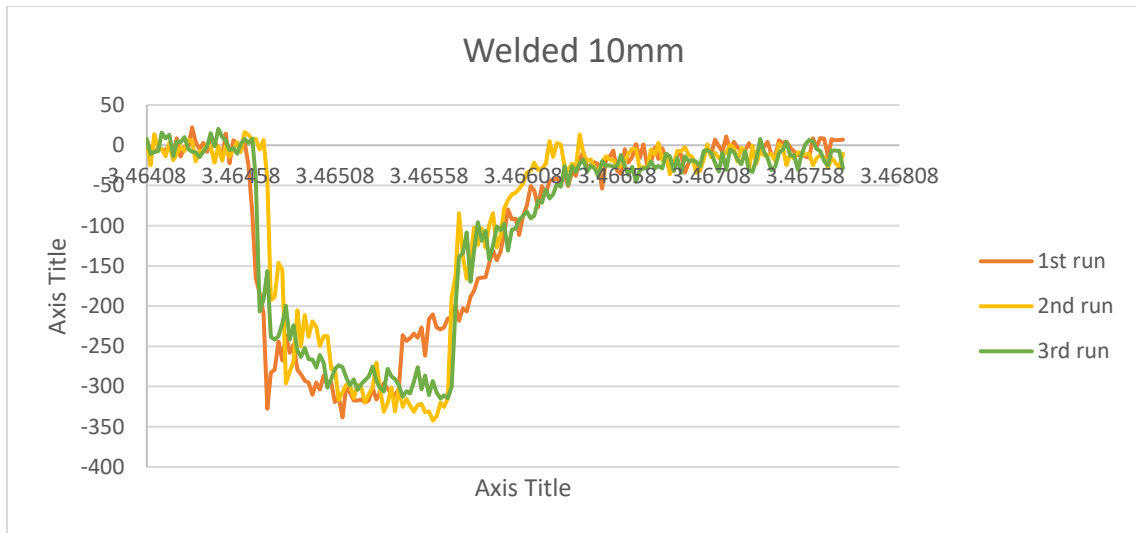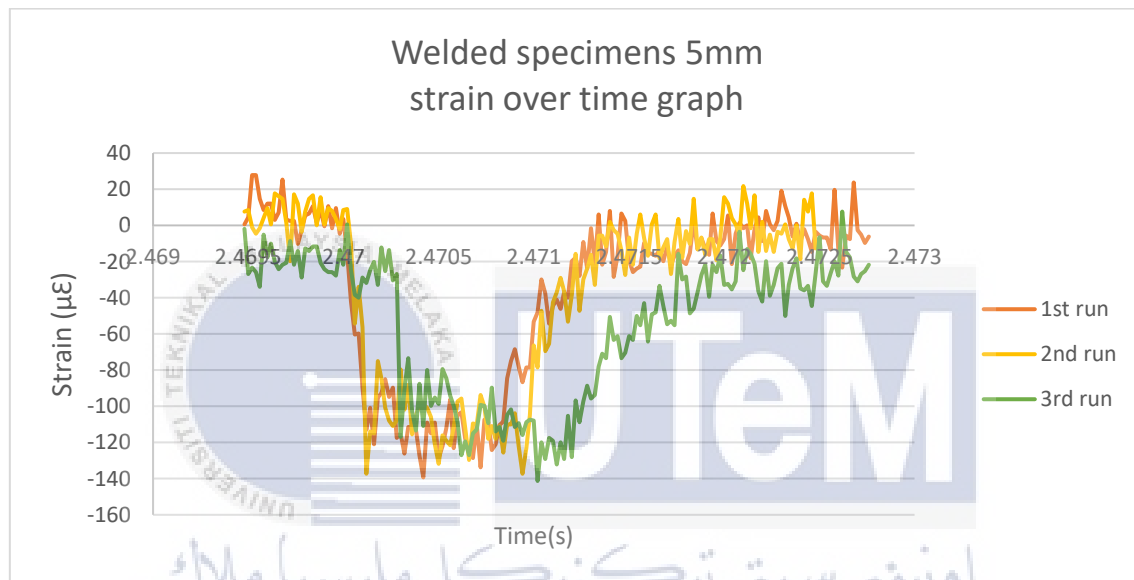

Figure 4.6 Welded specimens 5mm strain over time graph

Figure 4.6 displays a graph of the strain versus time signal for welded specimens with a thickness of 5 mm. The strain signal graphs from the first, second, and third runs are combined and stacked on top of one another. This demonstrates that the first and second test graphs produced nearly the same pattern, with the exception of the third run graph, whose impact duration is slightly longer than the other two. Regarding the strain value, all three graphs almost have the same range amplitude, which is almost as -150($\mu\mathcal{E}$).
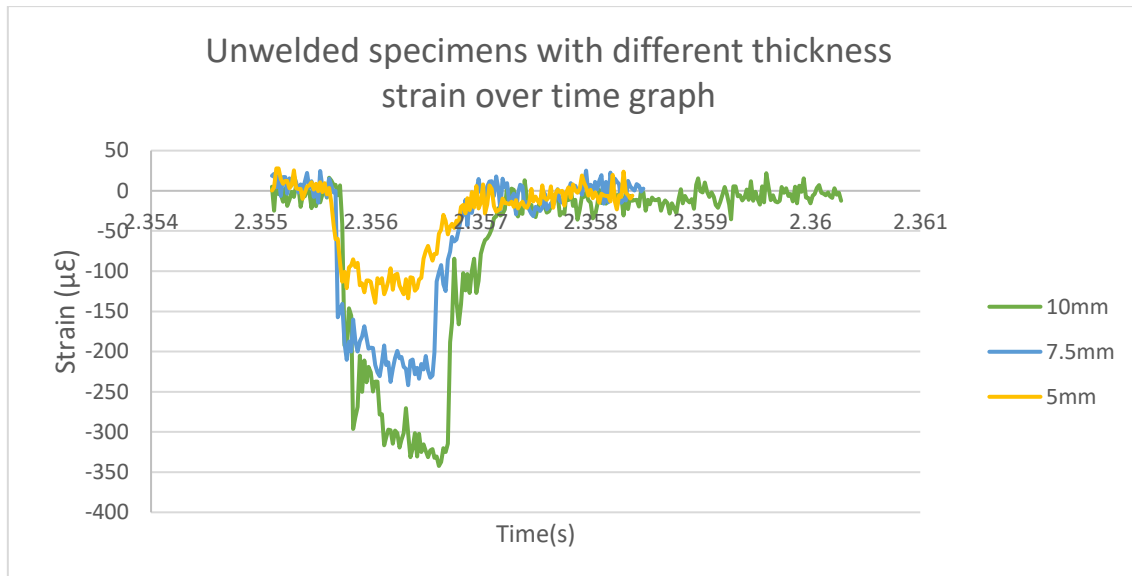
Figure 4.7 Unwelded specimens with different thickness strain over time graph

From the figure 4.7, the picture shows the graph of strain over time signal for unwelded specimens which has three different thickness which is 10mm,7.5mm and 5mm. the strain signal graph of those three different thickness is combined and stack upon each other. from this we can see that all three-graph produced almost the same pattern but differs in size. to elaborate more, the 10mm graph has the longer impact duration and strain of nearly -350(µƐ) which is the also the highest amplitude of them all. The 7.5mm graph has the second-longest impact duration and the second-highest amplitude, with a strain of around -250(µƐ). Last but not least, the 5mm graph has the smallest impact time and strain (close to -150µƐ), as well as the smallest amplitude among those three. This graph is valid through theory because when thickness of specimen was increased, the area under strain signal amplitude was increased that leads to higher impact time duration. (5)
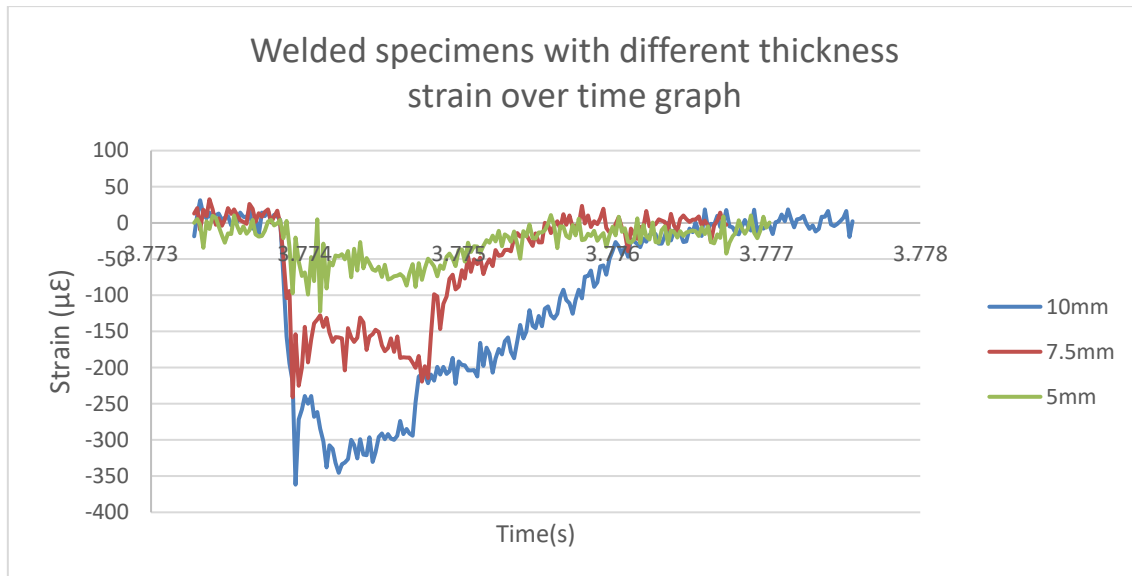
Figure 4.8 Welded specimens with different thickness strain over time graph

In figure 4.8, a graph of the strain versus time signal for welded specimens with three different thicknesses—10 mm, 7.5 mm, and 5 mm—is depicted. These three distinct thicknesses' strain signal graphs are mixed and stacked on top of one another. From this, we can see that all three graphs produced very comparable patterns, while varying in size, with the exception of the 10mm graph, which has a slightly different impact time curve. The strain signal's amplitude is at its peak for 10 mm thick materials and exceeds -350. In comparison to the other two thickness graphs, it graph also has the longest impact duration. For the 7.5mm thickness the amplitude of the strain signal is at the second which is nearly -250($\mu\mathcal{E}$). while so the graph has almost exact same impact duration with the 5mm thickness graph. Lastly, the strain amplitude is nearly -150 ($\mu\mathcal{E}$).on the 5mm graph, which has the lowest value.

4.3 Tensile Test

The ability of a material to endure an applied force or stress without failing or deforming plastically is referred to as a material's strength in terms of mechanics. A stress-strain curve is built to identify the material behavior of a material. The curve allowed for the

79

identification of yield, necking, and fracture point. The yield point marks the boundary between elastic behavior and the start of plastic deformation. The difference between the necking point and the fracture point is the point at which the material completely fails. Figure 4.9 and Figure 4.10 shows the force-displacement curve and stress-strain curve for heat treatment mild steel in this case the same material as the based material CVN specimen.

Based on Figure 4.9 and Figure 4.10, The material begins to yield at 0.2mm, producing an average elastic value of 17777.1MPa. it can be seen that the plastic deformation in the 3mm to 20mm range, also the max force of the material to withstand is with a stress at failure of 28kN on average. the break displacement at the peak is at the average of 24.5mm.
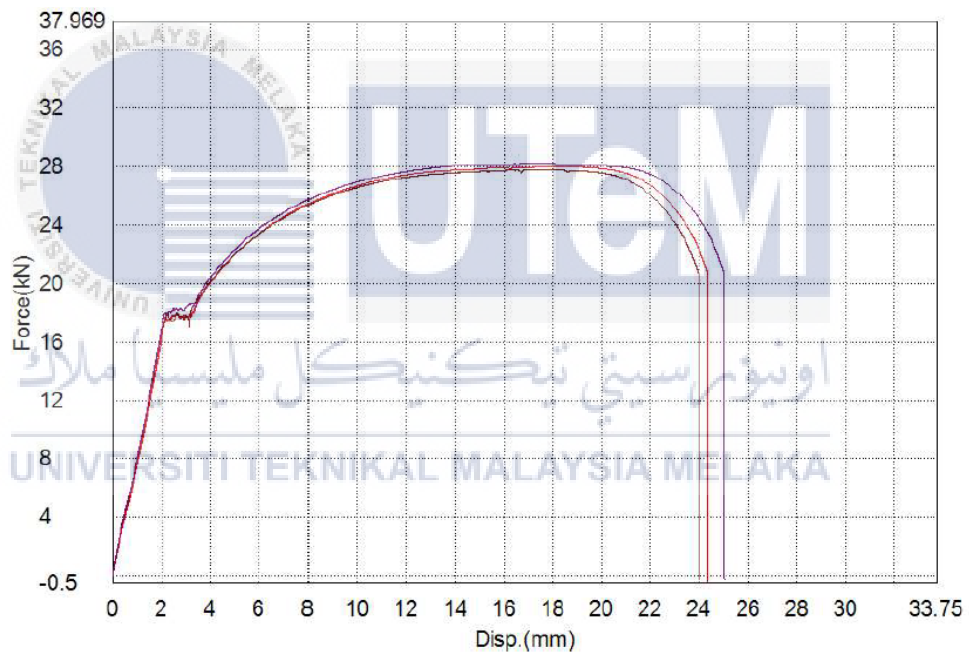
Figure 4.9 Tensile test force over displacement graph
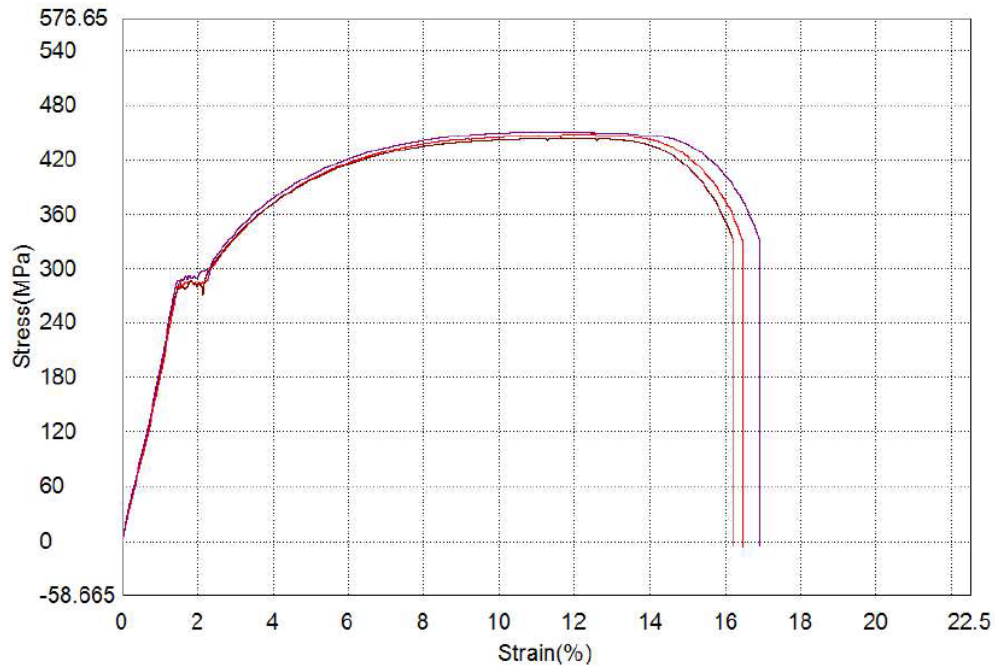
Figure 4.10 Tesnile test stress over strain graph

Additionally, the area under the stress-strain curve can be used to calculate the material's strain energy. To explore the energy held in a material under axial loading, strain energy is identified. Finally, a load-displacement (F-) graph is built to determine the material's yield, maximum and fracture loads as well as its absorbed energy. Due to the tensile test, energy absorbed was found to be a good indicator of material toughness. Table 4.8 shows the result of tensile load, max force, break displacement and energy absorbed for the material. Figure 4.11 shows the image of the specimen facture after the tensile testing is done.

Table 4.7 Tensile test recorded data

| Name | Max_Force | Tensile Strength | Elastic | Break_Disp. |
| Parameters | Calc. at Entire Areas | Calc. at Entire Areas | Force 1 – 5 kN | Sensitivity: 10 |
Unit	kN	MPa	MPa	mm
1	28.0584	447.859	17285.0	24.3514
2	27.8141	443.960	17740.5	23.9947
3	28.2460	450.855	18305.8	25.0172
Average	28.0395	447.558	17777.1	24.4544
Standard Deviation	0.21657	3.45735	511.384	0.51898
Maximum	28.2460	450.855	18305.8	25.0172
Minimum	27.8141	443.960	17285.0	23.9947
Range	0.43190	6.89502	1020.80	1.02250
Median	28.0584	447.859	17740.5	24.3514
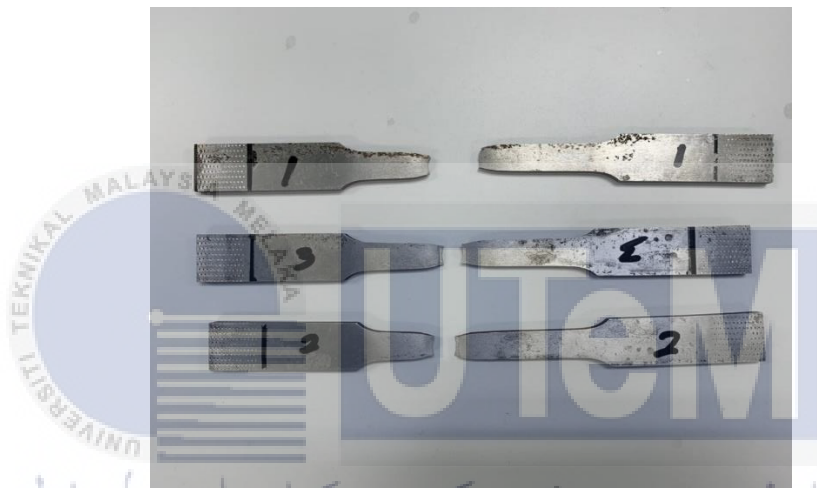
Figure 4.11 Tensile specimen after the fracture

4.4 Correlation Of Absorb Energy Between Welded and Unwelded Material

In this study, the energy absorbed is measured to investigate the material fracture toughness due to V-notch Charpy test at different parameters. The average energy absorbed from the impact test for welded material and unwelded material were shown in Table 4.9 respectively. Charpy V-notch results show that thickness and impact speed has influenced the material performance in energy absorption capability. The effect of thickness and amount of energy absorbed for both materials is demonstrated in Figure 4.12.

Table 4.8 CVN test energy absorb recorded data

Dimension		Unwelded (J)	Average(J)	Welded(J)	Average(J)
10mm	1.	90		125	
	2.	110	108.33	130	133
	3.	125		144	
7.5mm	1.	80		85	
	2.	82.5	79.17	82	82.33
	3.	75		80	
5mm	1.	62.5		50.	
	2.	62.5	63.33	45.5	49.33
	3.	65		52.5	

Figure 4.12 Energy absorb between welded and unwelded graph

From the table 4.9 the recorded energy absorbed value of CVN both welded and unwelded material is calculated for the average readings. Figure 4.12 shows a graph that was created using the average readings to compare the amount of energy absorbed by welded and unwelded materials of varying thicknesses (10 mm, 7.5 mm, and 5 mm). for the welded specimen, the 10mm thickness specimen has the highest energy absorb value, which is 133J,

83

followed by a thickness of 7.5 mm at 82.33 J and a thickness of 5 mm has the lowest energy absorb value which is 49.33J. The unwelded specimen's 10 mm thickness specimen likewise has the greatest energy absorption value, measuring 108.33 J, followed by 7.5 mm thickness, which comes in at 79.17 J, and 5 mm thickness, which comes in at 63.33 J as the lowest. As can be shown, the thickness of the CVN specimen has a direct correlation with how much energy it can absorb. As it can see the higher the value of thickness of the CVN specimen, the higher the value of absorb energy it receives. This is supported by impact studies, which shows that thinner materials that impact at high speeds are more easily damaged and fractured than thicker materials (Ali et al., 2013) [24].

Next, from the figure 4.12 shown. the value of different material which is welded and unwelded material also differs. As can be seen, the value of 10mm thick welded material is significantly larger than the value of 10mm thick unwelded material. Also, the same as 7.5mm thickness where the value of absorb energy of welded is slightly higher than the unwelded material. This is due to the fact that the welded material is exposed to significantly greater heat than the unwelded material (base metal), which slightly alters the material's properties. The chemical makeup of the filler metal and the process's heat input have a significant impact on the weld metal microstructure of fusion welded connections (Ragu Nathan et al., 2015) [30].

4.5 Analysis of Impact Signal Between Welded and Unwelded Material
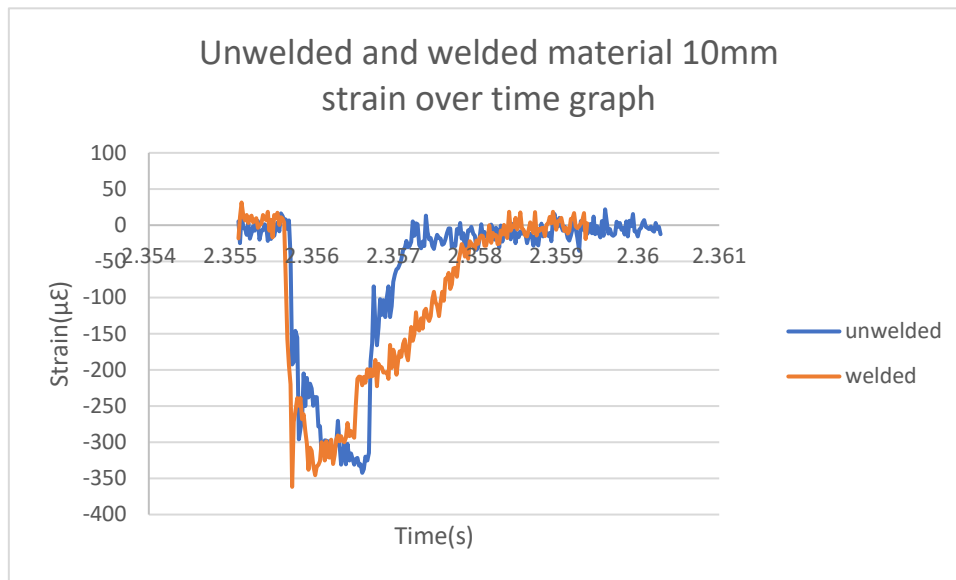
Figure 4.13 Unwelded and welded material 10mm

strain over time graph

Data from the unwelded and welded materials with a 10mm thickness strain signal graph are shown in Figure 4.13. For ease of signal data pattern comparison, these two graphs have been combined. In this instance, the welded material's strain amplitude value, which is -350($\mu\epsilon$), is higher than the unwelded material's, which is slightly lower below -350($\mu\epsilon$). It is also demonstrated that the welded strain signal graph had a longer impact duration 4ms compared to the unwelded material, which had a 3.18ms impact duration. As for under the curve area, the entire area of the unwelded material strain signal pattern's under-the-curve region is 0.35342m2. While the area that is welded under the curve is 0.45358m2, which is significantly larger. Figure 4.14 and Figure 4.15 shows the under the curve area for 10mm thickness specimen between strain over time graph respectively.

Figure 4.14 Under the curve area for unwelded 10mm

Figure 4.15 under the curve are for welded 10mm

Figure 4.16 Unwelded and welded material 7.5mm
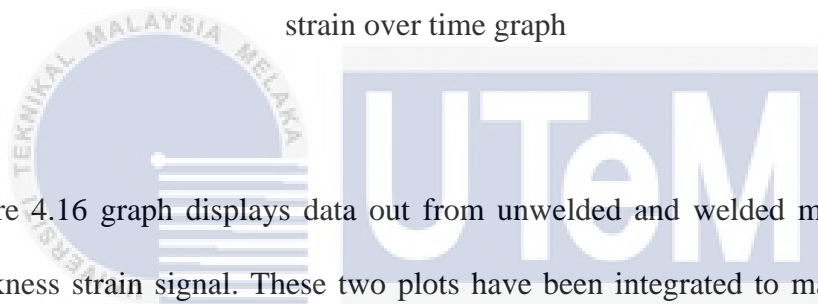
strain over time graph

Figure 4.16 graph displays data out from unwelded and welded materials with a 7.5mm thickness strain signal. These two plots have been integrated to make it easier to compare signal data patterns. In this case, the strain amplitude value of the unwelded material, which is close to -250(μƐ), is virtually identical to that of the unwelded material, which is also close to -250(μƐ). Furthermore, it is shown that the impact duration of the welded strain signal graph was slightly longer (2.46 ms) than that of the unwelded material (2.38 ms). The total size of the under-the-curve region of the unwelded material strain signal pattern is 0.20582m2. The area that is welded beneath the curve, however, is slightly smaller at 0.19604m2. The under the curve area for 7.5mm thick specimens between strain over time graphs is shown in Figures 4.17 and 4.18, respectively.
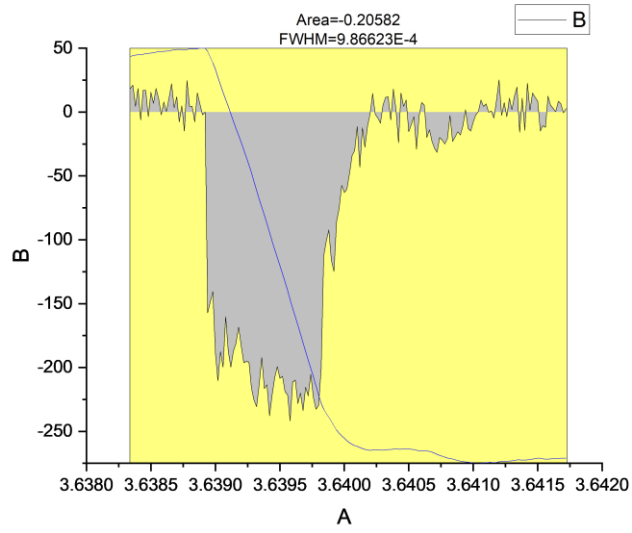
Figure 4.17 Under the curve area for unwelded 7.5mm
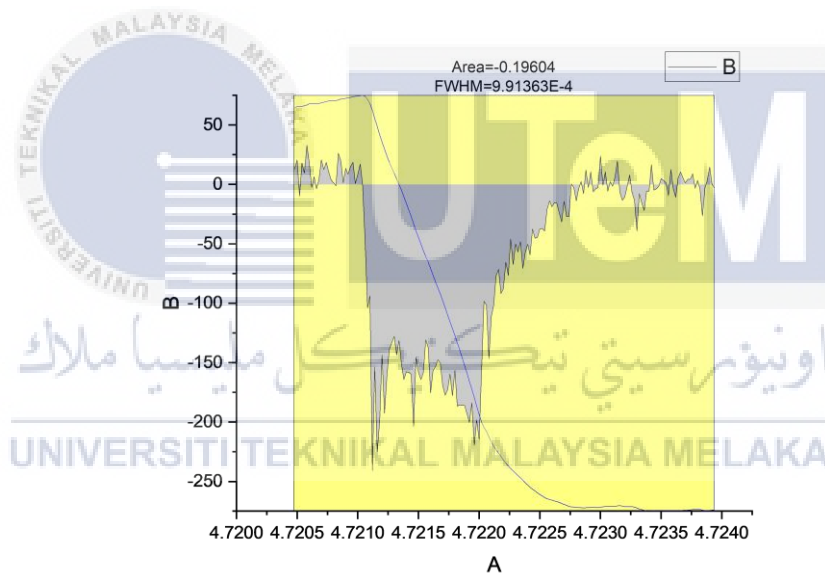
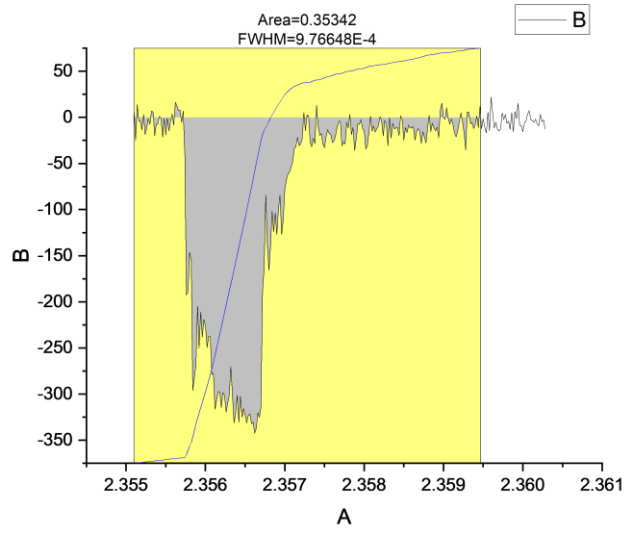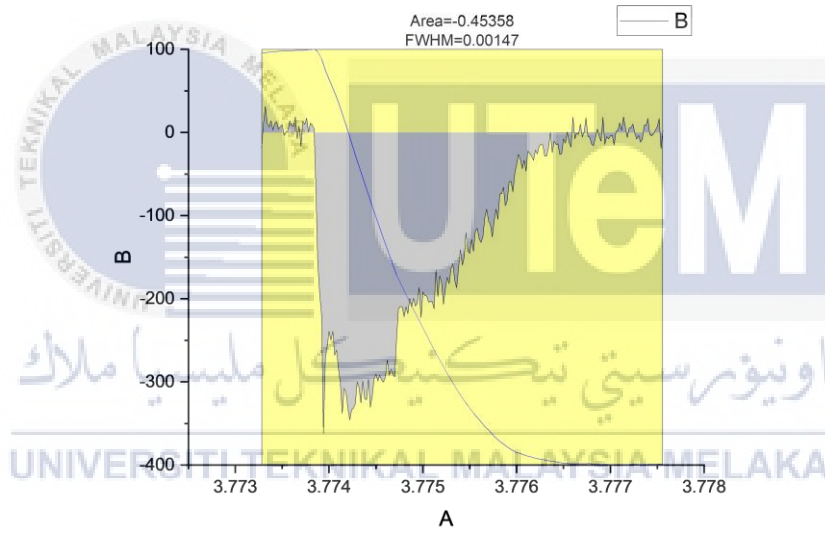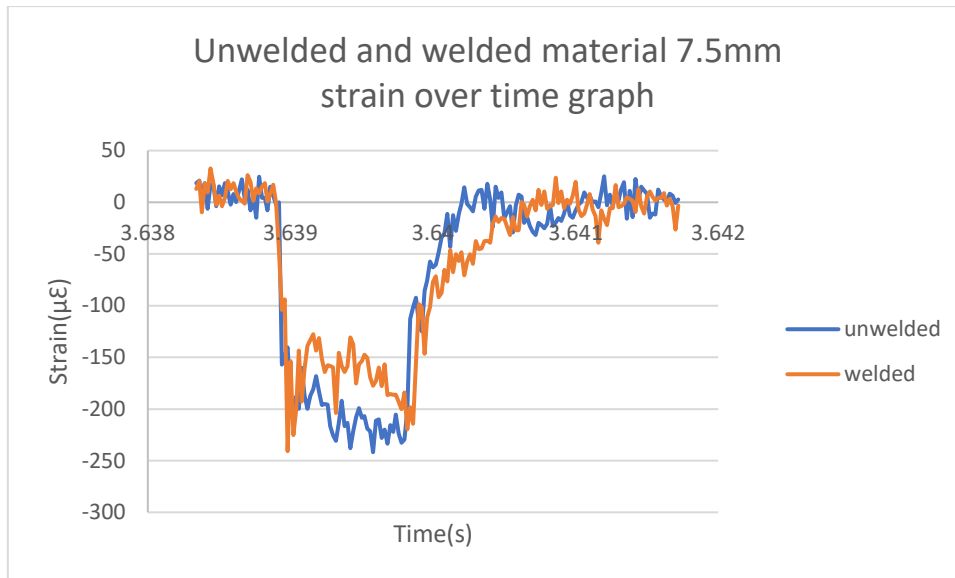Figure 4.18 Under the curve area for welded 7.5mm
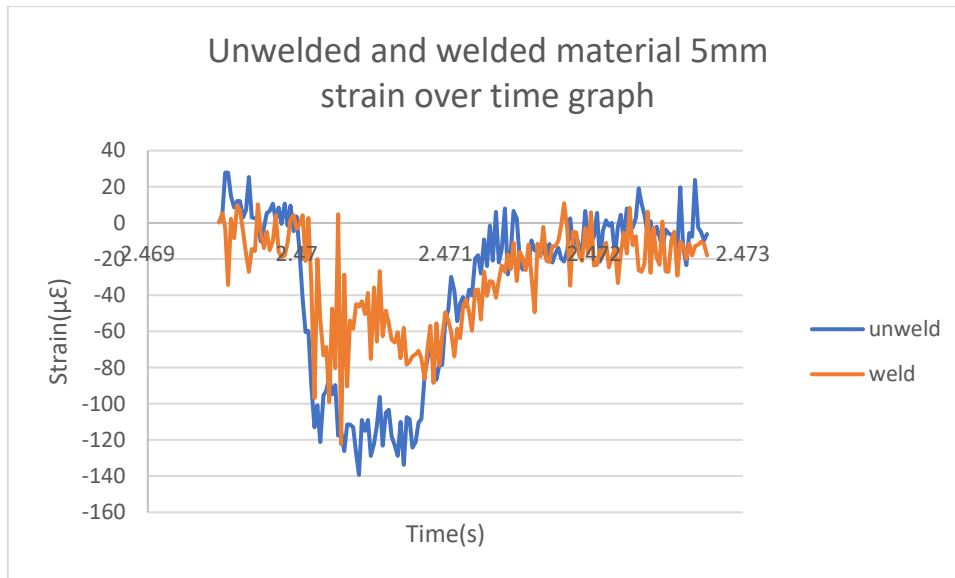
Figure 4.19 Unwelded and welded material 5mm

strain over time graph

Figure 4.19 displays data from the unwelded and welded materials with a 5mm thickness strain signal graph. These two plots have been combined for the purpose of simpler signal data pattern comparison. The unwelded material's strain amplitude value in this case is $-140(\mu\epsilon)$, which is larger than the welded material's value, which is just above $-120(\mu\epsilon)$. Furthermore, it is shown that the impact duration of the welded strain signal graph was longer 2.74 ms as opposed to 2.22 ms for the unwelded material. The under-the-curve portion of the unwelded material strain signal pattern spans the complete area of 0.11766m2. In contrast, the area that is welded beneath the curve is 0.10495m2, which is considerably less. Figures 4.20 and Figure 4.21, respectively, show the under the curve region for 7.5mm thick specimens between strain over time graphs.

89
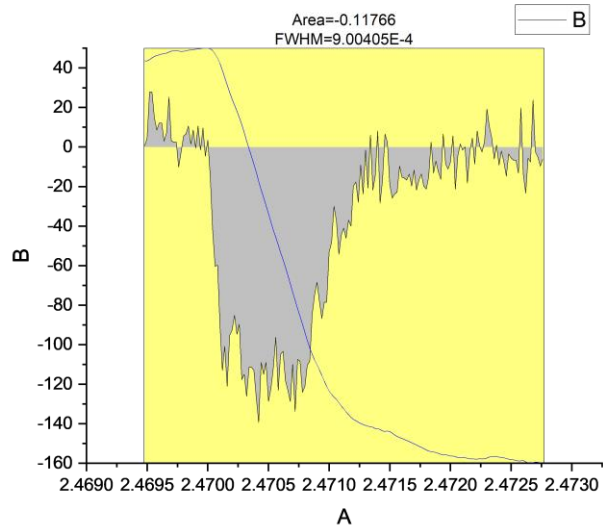
Figure 4.20 Under the curve area for unwelded 5mm
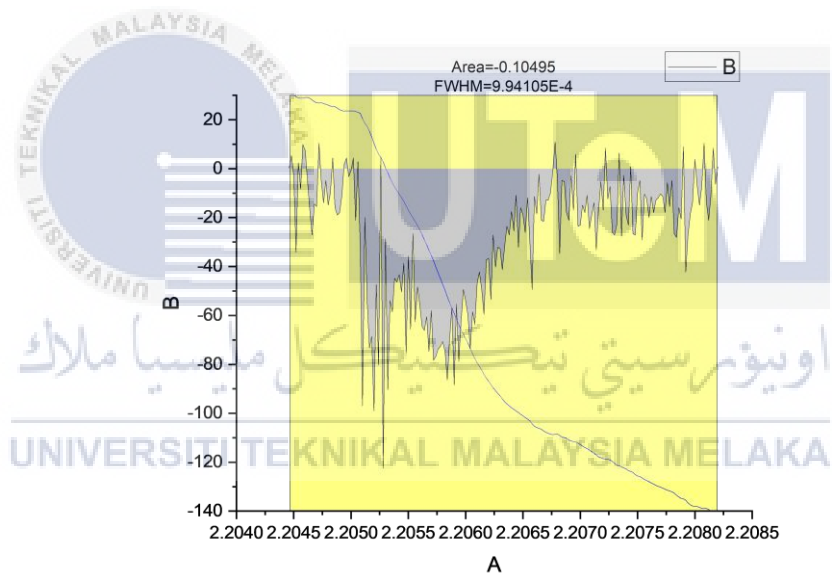

Figure 4.21 Under the curve area for welded 5mm

CHAPTER 5

CONCLUSION AND RECOMMENDATION

5.1   Conclusion

The results of this investigation show that thicker materials have the capacity to absorb greater impact energy. The least amount of energy is absorbed by thin materials that are struck with a high force. The area under the strain-time graph, maximum strain, and energy absorbed were all significantly influenced by the material's thickness. As a result, all of the Charpy test parameters aside from maximum strain are directly correlated with material thickness. The necessary time to shatter a test specimen is influenced by both thickness and kind of material. Although there are significant differences in impact length across experiment, theory, and earlier studies, the pattern is consistent. More time is required to fracture a thicker material compared to the thin material The area under the strain-time graph, the maximum strain, and the amount of energy absorbed are also affected by the type of material. In this instance, the research demonstrates that welded materials provide higher energy absorption and also demonstrate that they have a significantly longer impact duration than unwelded materials. Even though this study indicates that. The data from the strain signal also demonstrates that the peak strain value differs depending on the material thickness. Each of the materials also shows how various materials produce various graph patterns. Despite the situation, the data is still in the area where the value of welded and unwelded material is equivalent.

5.2   Contribution of study

Results of the Charpy V-notch test's impact strain signal have contributed to our understanding of material characteristics. To examine the stress-strain curve and forecast material behavior, the majority of research studies have used tensile tests. However, the form of the strain signal pattern from the Charpy test can be used in this study to determine the material behavior. Additionally, the instrumented Charpy test yields a number of results, including energy absorbed, maximum strain, impact duration, and area under the graph, which can be used to classify and categorize the test as a reference when a forecast is made. In light of the findings from mechanical testing of the instrumented Charpy test, this contribution represents a different approach to determining if a material is ductile or brittle.

5.3   Recommendation

Some suggestions are recommended to improve this study in future research. The suggestions are as follows: -

i.   Investigate the impact signal with the same type of welding and weld filler material but in different parameter. This idea is to show how different weld parameter can give an impact on material properties.

ii.   Investigate the impact signal with the same type of welding but with different filler material. this is to study the effect of different weld filler material on based metal.

iii.   A comparison of robotic welding machines against manual welding. How manually weld and robotic weld gives effect on impact signal.

REFERENCES

Bayraktar, E., Chevalier, J., Bonnet, F., Kaplan, D., & Claeys, J. (2009). Impact tensile test: A new type of crash test for welded joints used in automotive applications. *DYMAT 2009 - 9th International Conferences on the Mechanical and Physical Behaviour of Materials under Dynamic Loading*. https://doi.org/10.1051/dymat/2009032

Thomas, D. J. (2018). Analysing the failure of welded steel components in construction systems. *Journal of Failure Analysis and Prevention*, *18*(2), 304–314. https://doi.org/10.1007/s11668-018-0392-x

Oztas, A.G., 1999. Application of Impulse Momentum Theory to Vehicle Collisions. *Tr. Journal of Engineering and Environmental Science*, 23, pp.455–464.

RAJALINGHAM, C., & RAKHEJA, S. (2000). Analysis of impact force variation during collision of two bodies using a single-degree-of-freedom system model. *Journal of Sound and Vibration*, *229*(4), 823–835. https://doi.org/10.1006/jsvi.1999.2523

Goldsmith, W. (2001) Book on the Impact: The Theory and Physical Behaviour of Colliding Solids. Dover Publications, Mineola, 416 p.

Johnson, W. S., Masters, J. E., O'Brien, T. K., Delfosse, D., Pageau, G., Bennett, R., & Poursartip, A. (1993). Instrumented impact testing at high velocities. *Journal of Composites Technology and Research*, *15*(1), 38. https://doi.org/10.1520/ctr10352j

Britannica, T. Editors of Encyclopaedia (2021, November 16). conservation of energy. Encyclopedia Britannica. https://www.britannica.com/science/conservation-of-energy.

Johnson, Lee. (2022, June 4). How to Calculate the Force of a Falling Object. sciencing.com. Retrieved from https://sciencing.com/calculate-force-falling-object-6454559.html

Ashter, S. A. (2014). Characterization. *Thermoforming of Single and Multilayer Laminates*, 147–192. https://doi.org/10.1016/b978-1-4557-3172-5.00007-4

Saba, N., Jawaid, M., & Sultan, M. T. H. (2019). An overview of mechanical and physical testing of composite materials. *Mechanical and Physical Testing of Biocomposites, Fibre-Reinforced Composites and Hybrid Composites*, 1–12. https://doi.org/10.1016/b978-0-08-102292-4.00001-1

Sudin, V. V., Kantor, M. M., & Solntsev, K. A. (2020). Features of Weld Metal Brittle Fracture in Charpy tests. *Procedia Structural Integrity*, *28*, 1637–1643. https://doi.org/10.1016/j.prostr.2020.10.135

Kim, J. J., Pham, T.-H., & Kim, S.-E. (2015). Instrumented indentation testing and Fe analysis for investigation of mechanical properties in Structural Steel Weld Zone. *International Journal of Mechanical Sciences*, *103*, 265–274. https://doi.org/10.1016/j.ijmecsci.2015.09.015

Otani, M. (1957). Study of sensitivity of welded joints to cut at dynamic tests of double strike/J. Railway Engineering Research, 14(11), 503-529.
Hartbower, C. E., Orner, G. M. (1963). Metallurgical variables affecting fracture toughness in high-strength sheet alloys. Manlabs Inc Cambridge Mass.

Sirohi, S., Kumar, P., Gupta, A., Kumar, S., & Pandey, C. (2021). Role of ni-based filler on charpy impact toughness of the P91 welds joint. *Materials Today: Proceedings*, *44*, 1043–1049. https://doi.org/10.1016/j.matpr.2020.11.177

Sarna, S. K. (2015, November 21). *Steels for Automotive Applications*. IspatGuru. Retrieved June 4, 2022, from https://www.ispatguru.com/steels-for-automotive-applications/

Black, J. T., Degarmo, E. P., & Kohser, R. A. (2013). *DeGarmo's materials and processes in manufacturing / J. T. Black, Ronald A. Kohser*. John Wiley & Sons.

Banas, T. (2020, December 6). *How to calculate force of impact*. Sciencing. Retrieved June 4, 2022, from https://sciencing.com/calculate-force-impact-7617983.html

Cary, H. B. (2011). *Modern Welding Technology*. Prentice Hall.

Weman, K. (2012). *Welding Processes Handbook*. Woodhead.

Lincoln Technical Institute. (2021, June 4). *4 popular types of welding procedures*. Lincoln Tech News Blog. Retrieved June 4, 2022, from https://www.lincolntech.edu/news/skilled-trades/welding-technology/types-of-welding-procedures

Barbosa, V. S., de Godois, L. A. C., Bianchi, K. E., & Ruggieri, C. (2021). Charpy impact energy correlation with fracture toughness for low alloy structural steel welds. *Theoretical and Applied Fracture Mechanics*, *113*, 102934. https://doi.org/10.1016/j.tafmec.2021.102934

Kunigita, M., Aihara, S., Kawabata, T., Kasuya, T., Okazaki, Y., & Inomoto, M. (2020). Prediction of charpy impact toughness of steel weld heat-affected zones by combined micromechanics and Stochastic fracture model – part ii: Model validation by experiment. *Engineering Fracture Mechanics*, *230*, 106966. https://doi.org/10.1016/j.engfracmech.2020.106966

Ali, M. B., Zakaria, K. A., Abdullah, S., & Alkhari, M. R. (2015). Correlation of impact energy from instrumented charpy impact. *Applied Mechanics and Materials*, *815*, 221–226. https://doi.org/10.4028/www.scientific.net/amm.815.221

Silva, A. L., Varanis, M., Mereles, A. G., Oliveira, C., & Balthazar, J. M. (2018). A study of strain and deformation measurement using the Arduino microcontroller and strain gauges devices. *Revista Brasileira De Ensino De Física*, *41*(3). https://doi.org/10.1590/1806-9126-rbef-2018-0206

Shterenlikht, A., Hashemi, S. H., Yates, J. R., Howard, I. C., & Andrews, R. M. (2005). Assessment of an instrumented charpy impact machine. *International Journal of Fracture*, *132*(3), 297–297. https://doi.org/10.1007/s10704-005-4480-z

Kondryakov, E. A., Zhmaka, V. N., Kharchenko, V. V., Babutskii, A. I., & Romanov, S. V. (2005). System of strain and load measurement in dynamic testing of materials. *Strength of Materials*, *37*(3), 331–335. https://doi.org/10.1007/s11223-005-0046-6

Rittel, D., Pineau, A., Clisson, J., & Rota, L. (2002). On testing of charpy specimens using the one-point bend impact technique. *Experimental Mechanics*, *42*(3), 247–252. https://doi.org/10.1007/bf02410979

Madavi, K. R., Jogi, B. F., & Lohar, G. S. (2022). Metal Inert Gas (mig) welding process: A study of effect of welding parameters. *Materials Today: Proceedings*, *51*, 690–698. https://doi.org/10.1016/j.matpr.2021.06.206

Ragu Nathan, S., Balasubramanian, V., Malarvizhi, S., & Rao, A. G. (2015). Effect of welding processes on mechanical and microstructural characteristics of high strength low alloy naval grade steel joints. Defence Technology, 11(3), 308–317. https://doi.org/10.1016/j.dt.2015.06.001

APPENDIX A   GANTT CHART PSM1

Project Activity	2022														
	WEEK (PSM 1)														
	1	2	3	4	5	6	7	8	9	10	11	12	13	14	15
Problem statement, objective, and scope identification	BP Briefing	PLAN/ACTUAL													
Data collections (book, journals)								Mid Term Break							
Report writing-PSM 1(Chapter1)															
Report writing-PSM 1(Chapter2)															
Report writing-PSM 1(Chapter3)															
Report review 1															
PSM 1 report submission															
Presentation-PSM 1															
Study Week															
Final Semester Examination															
Semester Break															

🟥 PLAN

🟨 ACTUAL

97
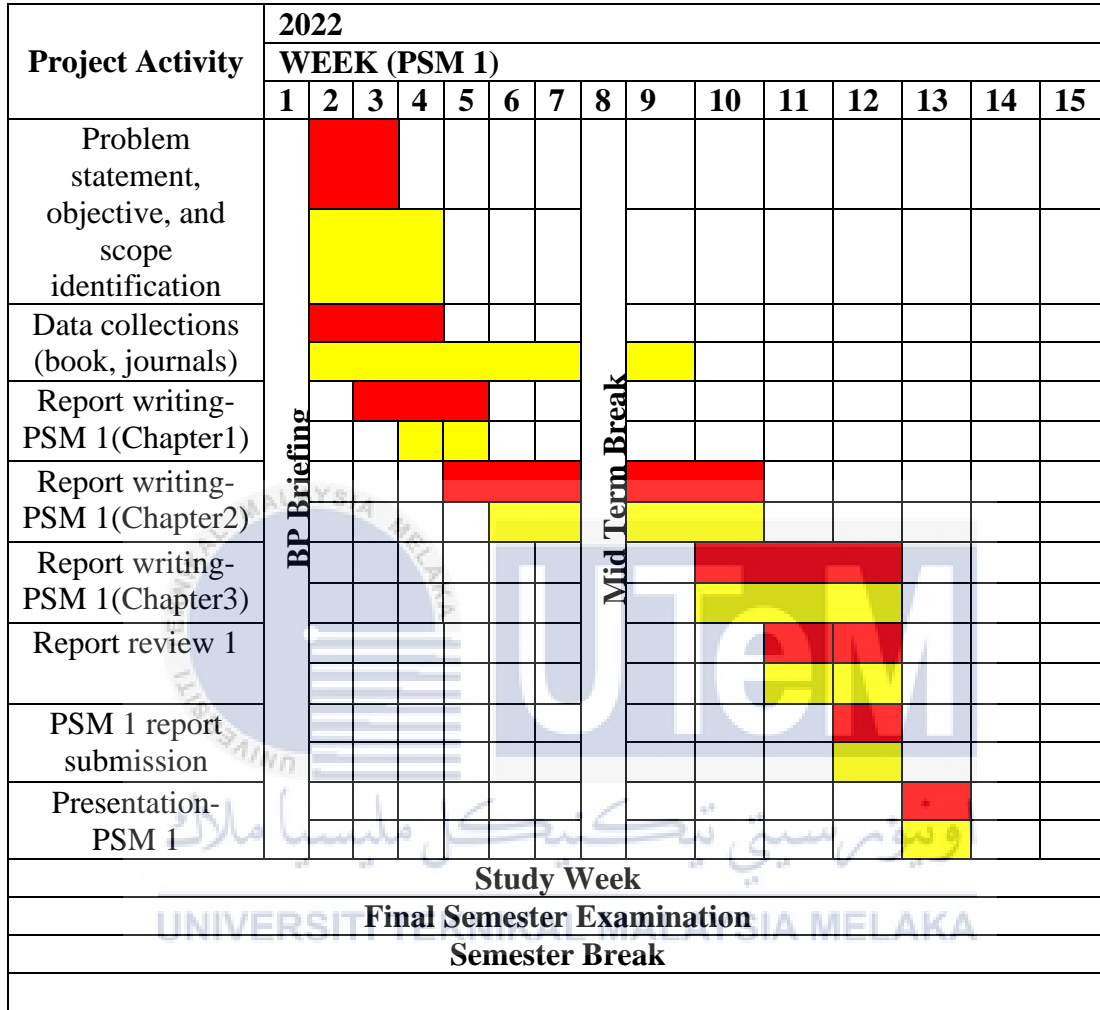
Project Activity	2022 WEEK (PSM 2)														
	1	2	3	4	5	6	7	8	9	10	11	12	13	14	15
Methodology Outline	BP Briefing	▮ (Plan) / ▮ (Actual)						Mid Term Break							
Build specimens			Plan 3–7 / Actual 3–7						Actual						
Experiment Conduct (Tensile & Charpy)									Plan 9–10 / Actual 9–11						
Result Data Analysed										Plan 10–11 / Actual 10–12					
Report writing-PSM 2(Chapter4)											Plan 11–12 / Actual 11–13				
Report writing-PSM 2(Chapter5)											Plan 11–12 / Actual 11–13				
Report review 1													Plan / Actual		
PSM 2 report submission													Plan / Actual		
Presentation-PSM 2														Plan / Actual	
Study Week															
Final Semester Examination															
Semester Break															

▮ PLAN

▮ ACTUAL

Chief Information Officer
Perpustakaan Laman Hikmah
Universiti Teknikal Malaysia Melaka

Melalui

Dekan
Fakulti Teknologi Kejuruteraan Mekanikal dan Pembuatan
Universiti Teknikal Malaysia Melaka

Tuan

PENGKELASAN TESIS SEBAGAI TERHAD BAGI TESIS PROJEK SARJANA MUDA

Dengan segala hormatnya merujuk kepada perkara di atas.

2.   Dengan ini, dimaklumkan permohonan pengkelasan tesis yang dilampirkan sebagai TERHAD untuk tempoh **LIMA** tahun dari tarikh surat ini. Butiran lanjut laporan PSM tersebut adalah seperti berikut:

Nama pelajar: ALI ZAINUL ABIDIN BIN KAMARUDIN

Tajuk Tesis: OBSTRUCTIVE SLEEP APNEA UPPER AIRWAYS MODELLING AND VALIDATION OF MANDIBULAR ADVANCEMENT SURGERY USING VARIABLE AIRFLOW AND THE EFFECT ON PRESSURE

3.   Hal ini adalah kerana IANYA MERUPAKAN PROJEK YANG DITAJA OLEH SYARIKAT LUAR DAN HASIL KAJIANNYA ADALAH SULIT.

Sekian, terima kasih.

"BERKHIDMAT UNTUK NEGARA"
"KOMPETENSI TERAS KEGEMILANGAN"

Saya yang menjalankan amanah,

NAMA
Penyelia Utama/ Pensyarah Kanan
Fakulti Teknologi Kejuruteraan Mekanikal dan Pembuatan
Universiti Teknikal Malaysia Melaka